BEAST II Technical Design Report DRAFT
For use in US Belle II Project TDR

Authors:

S. Tanaka, H. Nakayama, Y, Funakoshi,
KEK, Tsukuba, Ibaraki, Japan

T. Browder, I. Jaegle, S. Vahsen,
University of Hawaii, Honolulu, Hawaii 96822

D. Cinabro
Wayne State University, Detroit, Michigan 48202

F.H. Lin, M.Z. Wang,
National Taiwan University, Taipei City, Taiwan

C. Marinas
University of Bonn, Germany

May 31, 2013

Contents

1 Technical Description

1.1 SuperKEKB Commissioning Detector

1.1.1 US Role in a Background Commissioning Detector

The US Belle II groups have a lead role in the design, construction, and operation of the SuperKEKB commissioning detector (also affectionately known as BEAST II in the Belle II collaboration), which will characterize beam-induced backgrounds near the interaction point (IP), starting in Fall 2014. The commissioning detector is needed to prevent radiation damage to the Belle II detector, to provide feedback to the accelerator during commissioning, and to improve our simulation of beam induced backgrounds, which will be more important in Belle II than Belle due to the increased luminosity. The proposed work on the commissioning detector will be a natural continuation of our role during KEKB beam commissioning in 1997 and 1998, and allow the US groups to take a leadership role during a critical phase of the experiment, while requiring only modest investment in equipment and manpower. This is made possible by leveraging the historical involvement and technical expertise on radiation monitoring, gas/pixel tracking detectors, mechanical structures, and DAQ electronics in the US groups.

1.1.2 Commissioning Detector Motivation

Experience with KEKB, as well as PEP-II [2], has shown that during beam commissioning and vacuum scrubbing, it is critical to measure the particle and x-ray backgrounds near the interaction point in detail. Such measurements are needed to provide real-time measurements of luminosity and background levels to the accelerator group, to ensure a sufficiently low radiation level before the final detector is installed, and to tune the simulation of beam-related backgrounds that affect physics measurements in the Belle II detector. Due to higher beam currents and luminosity, beam-related backgrounds will be larger in Belle II than experienced in Belle. Due to the innovative nano-beam scheme employed by SuperKEKB, the relative contribution of different background components (e.g., beam-gas interactions, Touschek scattering, and synchrotron radiation) will also differ from that in KEKB. There are large uncertainties in the levels predicted by simulation, so that direct, *in situ* measurements of these backgrounds are needed.

1.1.3 KEKB Commissioning Experience

The Hawaii group led the KEKB commissioning detector effort in 1997 and 1998. The group provided the mechanical structure, drift tubes, and DAQ electronics for the BEAST (Beam Exorcism for a STable experiment) commissioning detector, shown in Fig. 1, and led installation and operation of this detector at KEK. BEAST detected the first KEKB beam in December 1998, the first Bhabhas, provided important feedback during the subsequent

accelerator commissioning, and provided data needed for tuning the simulation of beam-induced backgrounds in the Belle detector.

Detailed x-ray and neutron measurements were lacking in BEAST, but are clearly needed here: an unexpected synchrotron radiation component, due to a steering magnet that had not been simulated, burned a hole into the first Belle beampipe. During the initial KEKB operation there was also larger radiation damage to the first Belle silicon strip detector than expected, requiring early replacement of that detector system. Neutrons from beam backgrounds produced unexpectedly large backgrounds in the Belle KLM detector endcaps, increasing their dead time and decreasing their efficiency. Scaling to Belle II conditions, it was concluded that the resulting KLM performance losses would become unacceptable, which is why some of the KLM glass RPCs will be replaced with a with a scintillator-based design. This illustrates the significance of neutron backgrounds, and the importance of understanding their production. Neutrons also were an important unexpected background in the BaBar DIRC detector, and they are difficult to measure precisely.

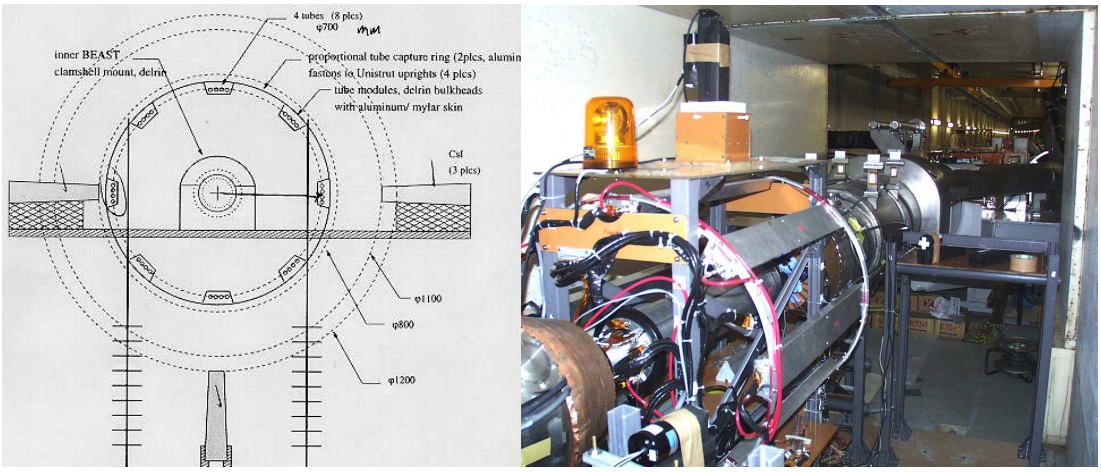

Figure 1: *Technical drawing (left) and photo (right) of the original KEKB beam commissioning detector, BEAST.*

1.1.4 Accelerator Group Goals / Motivation

Recently a consensus was formed on the commissioning scenario of SuperKEKB between the Belle II group and the SuperKEKB accelerator group. In this scenario, the commissioning will be performed in three steps.

In the first step (Phase 1) from January 2015 to May 2015, the machine commissioning will be done without the final focus quadrupole magnets (QCS's) and the Belle II detector. Instead, as shown in figures **??** and 3, a concrete shield will surround the area that will later become the interaction region. The main goals in this period are to complete the basic machine commissioning including the commissioning of each accelerator component

and to perform enough vacuum scrubbing before the Belle II detector is rolled in. Although no beam-collision will be done in this phase, some preliminary machine studies on more essential beam dynamics issues for a high luminosity will also be done such as low-emittance tuning. It is expected that the stored beam currents will reach $0.5 \sim 1$A in this phase. For increasing the beam currents, tuning of the beam feedback system for suppressing the beam instability will be important. The Belle II group requests that the vacuum scrubbing with $0.5 \sim 1$A for at least one month in total should be done. During Phase 1, the commissioning of the damping ring for the positron beam will also be done.

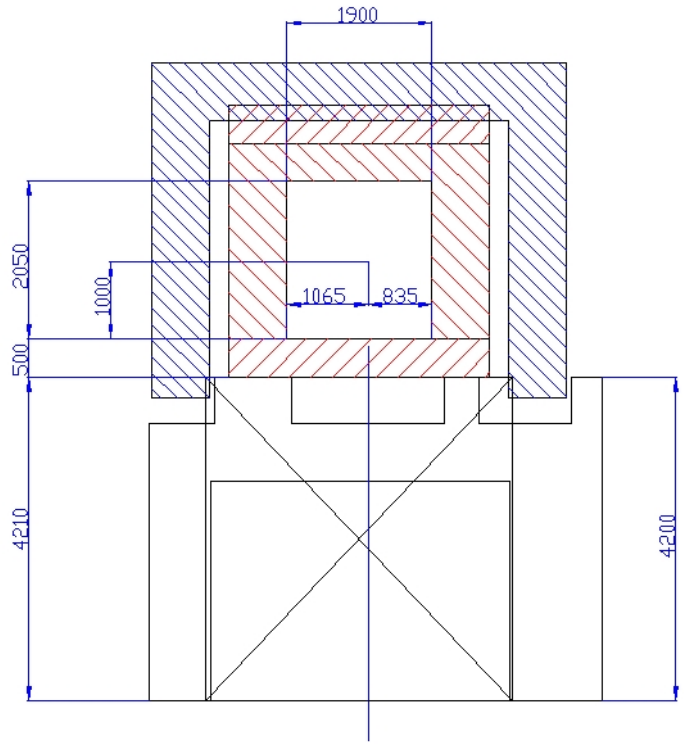

Figure 2: *Interaction region during commissioning phase 1, r/ϕ-view.*

In the second step (Phase 2) from January 2016 to April 2016, the accelerator commissioning will be done with QCS's and Belle II. Although the vertex detector will not be installed in this phase, the machine condition will be the same as that in the final stage from the viewpoint of the accelerator tuning and the full luminosity tuning will be done.

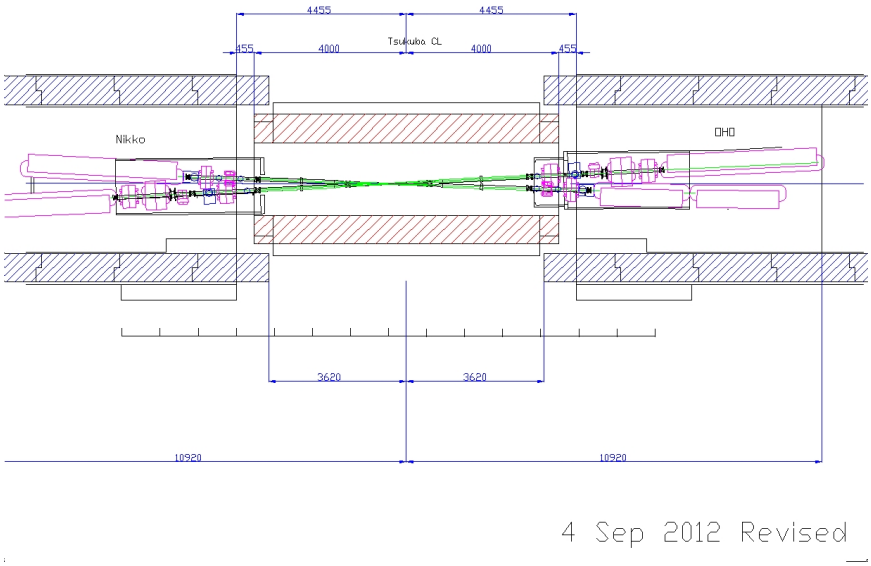

Figure 3: *Interaction region during commissioning phase 1, top view.*

The target luminosity at the end of this phase is $1 \times 10^{34}\mathrm{cm}^{-2}\mathrm{s}^{-1}$. Machine tuning in this phase includes optics tuning, beam collision tuning with the nano-beam scheme and tuning and the study on the detector beam background. As for optics tuning, the continuous orbit correction during the beam operation, tuning of squeezing the beta functions at the IP (low-beta tuning) and tuning on the low vertical emittance (low-emittance tuning) are important. Among them, low-beta tuning is essentially important in SuperKEKB and the achievable luminosity depends largely on the minimum value of the vertical beta functions at the IP. Squeezing the beta functions at the IP is not easy task and maybe we will need several years to attain or approach to the design values of the IP beta functions. As for beam collision tuning, the orbit feedback system to maintain the optimum beam collision and the beam tuning for suppressing the beam-blowup due to the beam-beam effects are important. In SuperKEKB, we will need a much faster orbit feedback, since the luminosity is much more sensitive to the motion of QCS's than the case of KEKB. As for the detector beam background, a realistic detector beam background will be studied before installation of the vertex detector. In SuperKEKB, there are three major sources of the detector beam background, *i.e.* the Touschek effect, the beam-gas Coulomb scattering and the radiative Bhabha process. The beam backgrounds from the Touschek effect and the beam-gas Coulomb are very sensitive to the IP beta functions. Since we will not reach the design values of the IP beta functions in this phase, we will need some extrapolation to estimate the ultimate beam background with the design machine parameters based on the study in this phase. The beam background from the radiative Bhabha process is not very sensitive to the IP beta functions and so the extrapolation to the design luminosity seems relatively straightforward. An example of the machine parameters corresponding to the target luminosity of $1 \times 10^{34}\mathrm{cm}^{-2}\mathrm{s}^{-1}$ is $\sim$ 1A in the beam currents, $\sim$ 2.4mm in the vertical beta function, which is 8 times larger

than the design, and ~ 0.025 in the vertical beam-beam parameter. The scenario mentioned above for Phase 2 is called the baseline scenario. In addition, we keep another scenario as a backup option where the commissioning in Phase 2 will be done with QCS's and without the Belle II detector in the case of some unexpected problems such as a delay in the Belle II construction.

In the third step (Phase 3) starting from October 2016, the full beam commissioning with the full Belle II detector will be done. At a some point in this phase, the physics experiment will start after some detector tuning, if needed.

1.1.5 Beam Background Sources at SuperKEKB

Major background sources at SuperKEKB are, Touschek effect, Beam-gas Scattering, Synchrotron radiation, Radiative Bhabha process, two-photon process, and beam-beam effect.

- Touschek effect

  Touschek effect is an intra-bunch scattering[7]. Coulomb scattering between two particles in a same beam bunch changes their energy to deviate from the beam bunch, one with too much and the other with too little energy. The scattering rate of the Touschek effect is proportional to the inverse beam size, third power of the beam energy, the number of bunches and second power of the bunch current.

  Touschek-scattered particles are lost by hitting the beam pipe inner wall while they propagate around the ring. If their loss position is close to the detector, generated shower might reach the detector. Fake hits generated by the background shower particles deteriorate the detector's physics resolution. In addition, radiation dose by gammas or neutrons in the background shower damage the Silicon devices used in the detector during the experiment.

  At SuperKEKB, simple extrapolation using the machine parameters predicts that Touschek background will increase by factor of $\sim$20 compared to that of KEKB. However, the background is reduced than this prediction because we introduce improved countermeasures.

  To cope with Touschek background, we install horizontal and vertical movable collimators. The movable collimators located along the ring can stop the deviated particles before they reach closer to the detector. The horizontal collimators are located at the positions where horizontal beta function or the dispersion become local-maximum. The horizontal collimators located just before to the interaction region play important role to minimize the beam loss rate inside the detector. The nearest collimator is only 18 m upstream of IP for LER. Touschek background can be reduced effectively by collimating the beam horizontally from both inner and outer sides. At KEKB, we had horizontal collimation only from inner side.

  The vertical collimator in LER, which is originally installed to reduce the Beam-gas Coulomb BG explained in the next subsection, also stops the vertically oscillating

Touschek scattered particles. Thoese particles are scattered at Fuji-area, which is opposite side of IP in the ring where LER beam orbit is vertically bending in order to pass under the HER ring.

- Beam-gas scattering

  The second background source is the beam-gas scattering by the residual gas atoms. Coulomb scattering changes the direction of the beam particle, and bremsstrahlung scattering decrease the energy of the beam particles. Scattering rate of the beam-gas scattering is proportional to the vacuum level and the beam current. At SuperKEKB, the beam currents will be $\sim$ 2 times higher than that of KEKB, and the vacuum level except for the interaction region will be the same level as KEKB. Therefore we have been expected the same order of magnitude (a few times higher) beam-gas background in the past publications[6]. However, our latest simulation study reveals that Coulomb scattering rate is higher by factor of $\sim$ 100 than that of KEKB, since IR beam pipe aperture is smaller and the maximum vertical beta function is larger. Beam-gas scattered particles are lost by hitting the beam pipe inner wall while they propagate around the ring, just like Touschek-scattered particles. The countermeasures used for Touschek background, movable collimators and the heavy-metal shield, are also effective to reduce beam-gas background. Especially, vertical movable collimator is essential to reduce Coulomb scattering background. Transverse Mode Coupling (TMC) instability caused by the vertical collimator should be carefully examined since vertical beta function is larger than horizontal beta function. Details are explained in [8].

- Synchrotron radiation

  The third background source is synchrotron radiation (SR) emitted from the beam. Since the SR power is proportional to the beam energy squared and magnetic field squared, the HER beam is the main source of this type of background. The energy of SR is few keV to tens of keV. At the first stage of Belle, the inner layer SVD was severely damaged by x-rays with E $\sim$ 2keV from HER. To absorb the synchrotron radiations before they reach the inner detector (PXD/SVD), the inner surface of the Beryllium beam pipe are coated with gold plate. The shape of IR beam pipe is designed to avoid direct SR hits at the detector.

- Radiative Bhabha process

  Photons from the radiative Bhabha process propagate along the beam axis direction and interact with the iron of the magnets. In these interactions, neutrons are copiously produced via the giant photo-nuclear resonance mechanism. These neutrons are the main background source for the outermost detector, the KL and muon detector (KLM) instrumented in the return yoke of the spectrometer. The rate of neutron production by the radiative Bhabha events is proportional to the luminosity, which is 40 times higher than that of KEKB. Therefore, additional neutron shield in the tunnel to stop those neutrons is installed.

  Both electron and positron energies decrease after radiative Bhabha process. If we employ the shared QCS magnets for incoming and outgoing beams as in KEKB, the

scattered particles are over-bent by the QCS magnets. The particles then hit the wall of magnets and electromagnetic showers are generated. In the SuperKEKB case, we use two separate quadrupole magnets and both orbits for incoming and outgoing beams are centered in the Q-magnets. We therefore expect the radiative Bhabha background due to over-bent electrons and positrons will be small and only a linmited fraction of them with very large energy loss(ΔE) are lost inside the detector. However, since the luminosity gets 40 times higher, those large ΔE particles are not negligible and will be comparable to Touschek and Beam-gas BG after installation of collimators. Beam intrinsic angular divergence at IP, angular diffusion by radiative Bhabha process, kick from the solenoid field, and leak field of the other ring's Q magnets (especially for electrons) play role for this radiative Bhabha background.

- Two-photon process

  The fifth background source is very low momentum electron-positron pair backgrounds produced via the two-photon process: $ee \rightarrow eeee$. In SuperKEKB, the radius of the innermost detector is less than that of KEKB since we introduce the pixel detector close to the IP. The two-photon background rate increases roughly as $1/r^2$. MC simulations and machine studies at KEKB in 2010 has shown that the two-photon BG rate on the PXD is less than our requirement. As of Feb. 2012 we suffered from the discrepancy between SuperB's results. However, after the face-to-face discussion in joint BG Workshop in Vienna, this discrepancy has disappeared and we both agree that our number is correct.

- Beam-beam background

  A beam bunch interacts with the electric field of the other bunch when they collide at the IP. A beam particle is kicked by this interaction and the kick force is almost proportional to the distance from the center of the bunch at $x/\sigma << 1$. Beam-beam interaction results in non-Gaussian shape of beam tail, therefore it might increase the background rate such as synchrotron radiation. Simulation study is performed using huge CPU power needed for a non-linear force calculation. Non-Gaussian tail is significant only for the vertical beam size, and the synchrotron background is not affected much.

The BEAST group is currently planning the following measurements:

Phase 1, Vacuum scrubbing phase:

- Measuring beam gas backgrounds in order to extrapolate background condition tot he target vacuum level
- Measuring injection noise / background rate and its time profile for both LER and HER

Phase 2, Belle without VXD:

- Measuring beam gas backgrounds in order to extrapolate background condition tot he target vacuum level
- Measure the Synchrotron (SR) hit rate on the PXD sensor area in order to feedback expected PXD operation condition, and decide on the beam abort setting of the VXD . If we find significantly larger SR background hit rate than expected, the beam pipe inner structure may have to be modified in order to meet the PXD required level. Such feedback is very important for safe operation of PXD during the physics run.
- Measure Touschek background by changing beam size with same bunch current. By monitoring neutron and electromagnetic shower hits during this study, we can validate the background simulation and can estimate background conditions during the physics run.
- Touschek and radiative bhabha backgrounds will be measured not only by BEAST II subsystems, but also via the CDC HV current and hit rate information from the Belle II TOP and ECL subdetectors. In particular on for TOP, the rate of background hits dye to radative bhabha events may be critical for the lifetime of the MCP-PMTs used in that detector. If we measure larger background levels than expected, additional shielding will be adopted before starting the physics run.
- Measure the effect of movable masks. In order to efficiently reduce background around the interaction region, SuperKEKB will employ movable masks. Measuring the background level as a function of mask position is useful fundamental data for optimizing the mask settings for the physics run.

1.1.6 Commissioning Detector Description and US Contributions

The US Belle II groups will design and build the following commissioning detector components: the mechanical support structure for mounting subdetectors, a PIN-diode array for monitoring radiation dose from charged particles and x-rays, and micro Time Projection Chambers for monitoring neutrons.

A range of (non-US) collaborating institutes will install other detector prototypes and subsystems on the commissioning detector, such as silicon strip and pixel detectors, a drift chamber prototype, and a BGO crystal-based luminosity monitor.

1.1.7 Commissioning Detector Design and Simulation

Figures 4 and **??** show the SuperKEKB commissioning detector design for commissioning phases 1 and 2, respectively. The instantaneous and integrated radiation dose throughout the inner detector volume will be monitored with an array of 64 PIN diodes. Neutrons will be monitored with an array of eight micro Time Projection Chambers (micro-TPCs). Eight sets of BGO calorimeter crystals will be used for luminosity monitoring.

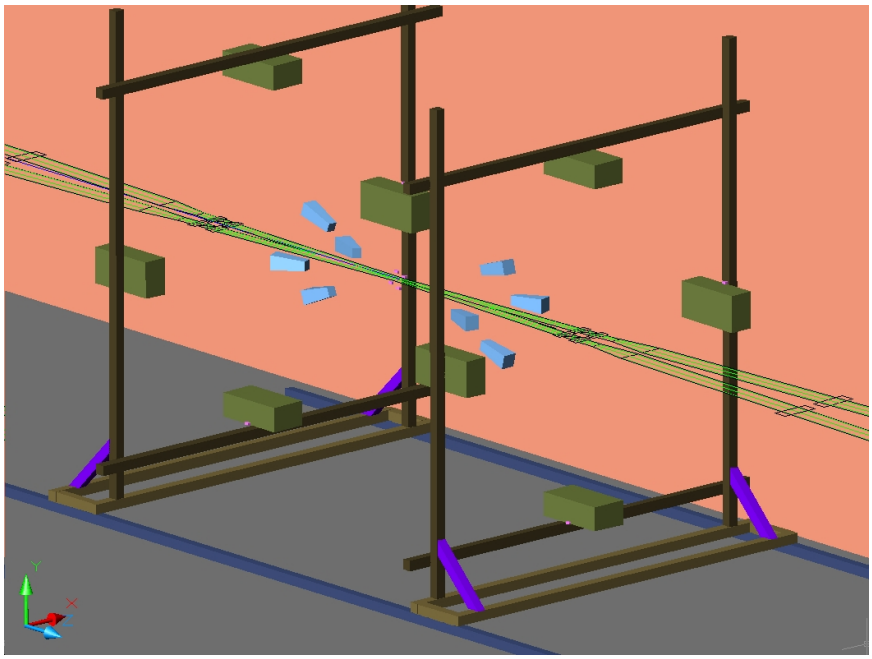

Figure 4: *Commissioning detector during phase 1.*

During commissioning phase 1 the different monitors will be mounted on a common mechanical structure, which is expected to be similar to that of BEAST used in Belle, shown in Fig. 1, but must now fit within the ECL calorimeter radius. Due to the proximity of accelerator magnets, non-magnetic materials such as fiberglass-based "Unistrut" support beams and brass connectors are required throughout. The most important system during this phase is the diode sytem, which will tell us when radiation levels are suffciently low that it is safe to roll in Belle II. During phase I we expect to install only two of the microTPCs, and to operate the BGOs in analog readout mode. While the BGOs and TPCs are not critically needed during this phase, they provide complimentary information on backgrounds, and operation during phase I will allow us to perform systems tests that ensure smooth operation of the BGO and TPC sytems during phase II.

Another motivation for having the BGO and TPC systems ready early, is the possbility of an alternate commissioning scneario: In that case the the Belle II construction schedule slips, it has been discussed that the QCS magnets would be installed before Belle II is rolled in. In that case the accelerator is likely to produce measurable luminosity and significant beam backgrounds of all major types, while there would much space available for BEAST II susbsystems mounted on the same support structure as used during phase I. Having the BGO and TPC systems operational during the QCS-but-no-Belle-II phase should allow useful measurements of all beam background components. While this is a backup-scenario that is not part of the default schedule, our group has been charged to be ready for all possible commissioning scnearios, including this one.

During phase 2 all Belle II detectors except the vertex detectors (VXD) will have been

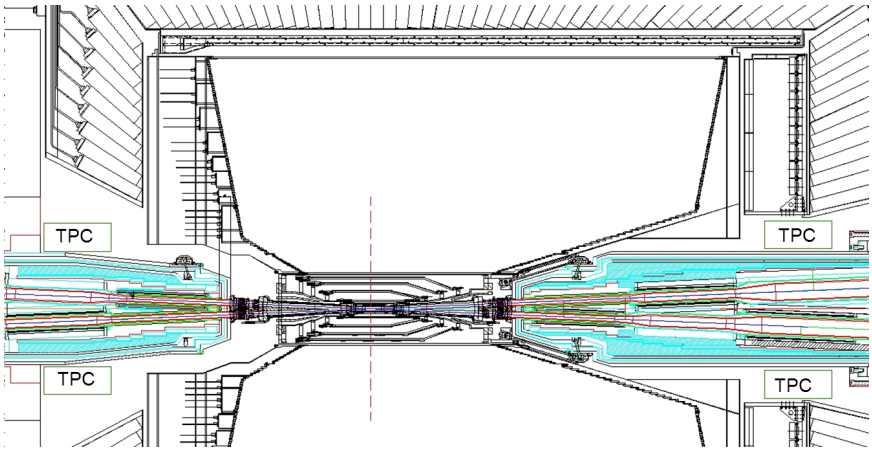

Figure 5: *Commissioning detector during phase 2.*

installed, so there is little space available for BEAST systems. At that time, the PIN diodes will be installed througout the VXD volume, the BGO system will be mounted on aluminum rings inside the VXD volume, while the eight TPCs will be installed in the SVX dock space. This space is reserved for VXD cabling boxes, and will thus still be available. At the same time the dock space happends to be particulary suitable for measuring beam backgrounds, as a significant fraction of critical beam backgrounds that e.g. affect the PID system are generated by beam particles hitting the beam pipe wall near the z-location of the forward and backward dock spaces, with a high rate of neutrons expected to traverse the dock space. The VXD group plans for phase 2 are still under discussion. The current expectation is that they will install two prototype pixel detector (PXD) ladders, two silicon vertex detector (SVD) ladder, and a range of specialized sensors for characterizing synchrotron radiation and background rates, as described below.

Members of the Hawaii group, led by Professor Vahsen, will perform simulations of the beam backgrounds expected during the commissioning period. They will work closely with KEK and the other groups involved to iterate the design of the commissioning detector, including the placement of subsystems, the mechanical support structure that positions these subsystems, and the shielding to protect the Belle II calorimeter. In order to produce the current conceptual design on very short notice, the Hawaii group started out by analyzing the existing beam background Monte Carlo simulation (an effort lead by Dr. Nakayama at KEK), which assumes the final SuperKEKB design parameters for the beams, and the final Belle II detector geometry. First results from this analysis (discussed below), combined with simple scaling arguments and conservative assumptions, provided good initial design guidance, but also have large uncertainties. The group will proceed to implement a dedicated GEANT geometry based on the commissioning detector conceptual design, and run a revised background simulation that assumes commissioning beam conditions. This should provide a more firm estimate of the background rates expected during commissioning and will allow us to refine the conceptual design into a technical proposal. Future simulations should include beam-gas bremsstrahlung, which is not included in the most recent background simulations,

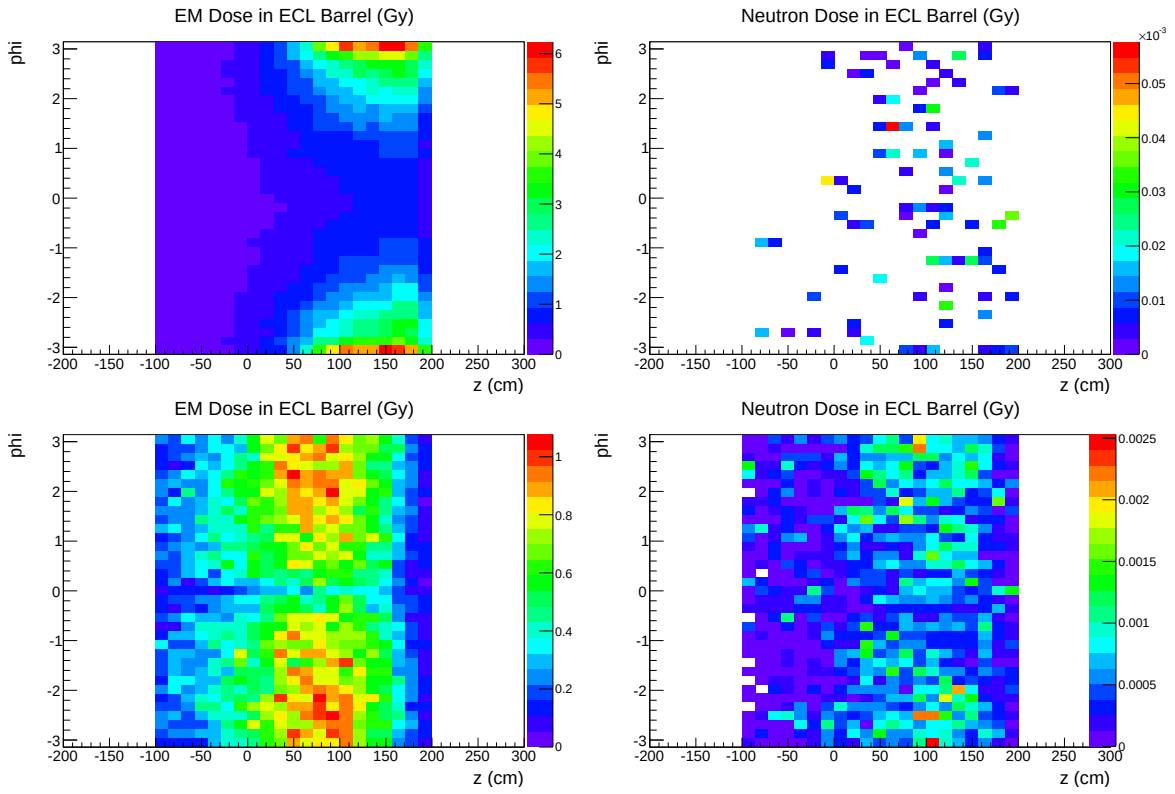

Figure 6: *Expected radiation dose in the electromagnetic calorimeter barrel from per snowmass year (10^7 seconds) of running at SuperKEKB design luminosity, extrapolated from simulating 20 μs of accelerator operation. Upper plots show radiative Bhabha events originating from the high energy electron ring (HER), while the lower plots show beam-gas Coulomb events originating from the low energy positron ring (LER).*

but may be important during commissioning.

Figure 6 shows the radiation dose deposited in the electromagnetic calorimeter (ECL) by two beam background processes during 10^7 seconds (one snowmass year - an upper limit on the commissioning period) of accelerator operation at SuperKEKB design luminosity. Table 1 shows the corresponding radiation dose for all simulated background processes, averaged over the whole calorimeter barrel. For reference, a dose of order 10 Gray (=1 krad) can start to degrade calorimeter performance.

At design luminosity and design beam conditions, radiative Bhabha events contribute the largest dose. More than 99% of the total ECL dose is due to electromagnetic (EM) radiation (x-rays, electrons, and positrons), with the remainder being deposited mainly by neutrons, protons, and pions. Since neutrons require a different shielding strategy than the other particles, and because of the Belle detector's vulnerability to neutrons, we usually separate out the neutron component when quoting simulation results. Both EM particles and neutrons that end up in the ECL originate primarily from the QCS magnet regions,

	Total Dose (Gy)	EM Dose (Gy)	Neutron Dose (Gy)
Coulomb (beam-gas) HER	0.002	0.002	0.0000
Coulomb (beam-gas) LER	0.306	0.296	0.0003
Radiative Bhabha HER	0.574	0.573	0.0000
Radiative Bhabha LER	0.131	0.131	0.0002
Touschek HER	0.005	0.005	0.0000
Touschek LER	0.440	0.438	0.0003
Total	1.458	1.445	0.0008

Table 1: *Expected average dose in the electromagnetic calorimeter from beam backgrounds, per snowmass year (10^7 seconds) of running at SuperKEKB design luminosity, at a vacuum pressure of 10^{-9} Torr (simulation).*

where the beams are strongly focused. These conclusions hold for all simulated backgrounds types, and they are expected to hold for commissioning conditions. During commissioning, however, there will be much lower luminosity, less focused beams, smaller beam currents, and a much worse vacuum. As a result it is expected that the radiation dose will be completely dominated by beam-gas events. There is no trivial way to scale the dose calculated during design conditions to commissioning conditions. The vacuum can easily be three orders of magnitude worse, leading to three orders of magnitude higher dose for the same beam conditions. In that (hypothetical, since the beam conditions will differ) case the total dose from beam-gas Coulomb events would be of order 30 Gray for an average ECL crystal per month of running with 30% duty cycle. Since the calorimeter dose is not uniform, the hottest crystals would receive a dose that is up to three times larger. This could endanger the calorimeter. To illustrate that the radiation levels can be severe during commissioning; the highest radiation dose rate seen during KEKB/Belle commissioning was 0.25 mGy *per second*, i.e. much higher than the beam-gas dose rate predicted for SuperKEKB design luminosity and 10^{-9} Torr vacuum pressure.

In conclusion, at present there is some guidance from simulation regarding the composition and origin points of beam-induced backgrounds, but the normalization is very uncertain. Shielding of the calorimeter against EM particles from beam-gas events may be required during the commissioning period. The conceptual design includes high-Z (lead) shielding that extends well past the QCS hot spots around $z = \pm 1$ m. The drawing shows the thickness of the lead shield as 2.6 cm, or 4.6 radiation lengths, which would reduce the EM dose by a minimum of 2 orders of magnitude. Fast neutrons are not strongly affected by the EM shield, and the stopping of charged particles in the EM shield is likely to result in additional neutron dose in the calorimeter. Hence the conceptual design also includes 10 cm of borated polyethylene to moderate and capture neutrons. This would reduce the dose from neutrons by approximately one order of magnitude, so that it remains small compared to the dose from EM radiation. The thickness of both shields will be adjusted as we refine our simula-

tions. It is possible that only the EM shield will be needed, so that the conceptual design, which includes both EM and neutron shielding, is conservative.

1.1.8 Commissioning Detector Dose Monitor

A simple, cheap robust monitor of ionizing radiation is an array of silicon PIN diodes. Ionizing radiation effectively causes an increase in the dark current from such diodes. This current can be passively amplified and its integral is proportional to the ionizing radiation dose. Such a system was used at CLEO and CESR to monitor and as a beam tuning aid to minimize beam induced radiation. At CLEO half of the diodes were behind a thin layer of high-Z shielding, a layer of gold paint, and half were unshielded. X-rays from synchrotron radiation are considerably reduced on the shielded diodes while particle radiation from beam-gas scattering and radiative Bhabha events is not. Thus the difference between a shielded and unshielded diode pair gives a direct measure of the synchrotron radiation component of the dose. At CLEO and CESR this made it easy to map the location and extent of synchrotron radiation and backscattering fans caused by the beams passing through the final focusing elements and x-rays scattering off of shielding elements.

A prototype system has been demonstrated at Wayne State. It uses commercial amplifiers from Cremat, Inc. and off the shelf PIN diodes from Siemens. The system returns the expected current when irradiated by a beta source of known activity. Work is going on to make the system multichannel, the commercial preamps are single channel, by sharing input power among many amplifiers.

A single diode is packaged into an aluminum block with a hole drilled out that leaves the sensitive face of the diode exposed along a long side. The leads of the diode are then attached to coax cable making for a very small, 1X1X2 cm, light package that can easily be held in place with velcro straps. They are also easy to move around with minimal effort. A pair of two, one with a bare window and a second behind a high-Z layer, form the basic sensor. Four pairs, up, down, inside ring, outside ring, form a basic measuring unit at a single location along the beam line. We plan to manufacture eight such units for a total of 64 diodes.

During the T0 phase we want a flexible system that we can move around in response to improving beam vacuum, changing beam conditions, and for machine studies. Also we would like two units of diodes to accompany the TPC's as a cross check of the ionizing dose they are observing. The remaining six units would be spread along the central beam line to monitor the radiation coming from the beam line.

During the T1 phase two units remain with the TPC's while the remaining six are placed on the outside of the final focus quads. Our simulations of the beam induced backgrounds show that the most troublesome radiation is coming from the quads and the diodes will provide a direct measure and test of the simulations.

During the T2 phase the diodes will move the inner tips of the ECL, where the largest dose on the calorimeter is expected, at the inner face of the quads, and the remaining four

units in the VXD volume to monitor dosage there.

This system will give us a low resolution view of any sharp x-ray features incident on the beam pipe at the longitudinal position of a diode unit. These radiation features get broadened as they scatter out of the beam pipe, thus making a higher resolution view not useful. We expect, based on the simulations of the backgrounds, that those diodes in the plane of the rings would see x-ray features while those out of the plane would not.

The diode signals would be brought to remote analog amplifiers on shielded co-axial cables. Keeping the amplifiers remote allows us to adjust the gain as the dose regime changes during the scrubbing and beam tuning processes. We would emulate the CLEO and CESR experience in having a low and high gain output, useful for monitoring and tuning during injection versus normal running, giving the system robustness and flexibility. We plan to take advantage of existing KEK infrastructure to digitize the analog diode signals. Since we envision these radiation monitors to be useful in beam tuning, they will be made available in real-time to the KEKB control room.

The sensors, cables, and mounting hardware will be constructed at Wayne State using the groups in-house technical support. Members of the Wayne State group, led by Professor Cinabro, will oversee the construction, installation, and commissioning of this sub-system, and analyze the resulting data.

1.1.9 Commissioning Detector: PXD group plans

Given the proximity of the Belle II DEPFET pixel detector (PXD) to the beams, it is especially vulnerable to beam backgrounds. The commissioning efforts of the PXD group are led by Dr. Marinas of Bonn University. The PXD group favors a two-stage commissioning scenario, where the silicon detectors (PXD and SVD) will be installed after beam pipe vacuum scrubbing and machine tuning, in order to prevent or limit radiation damage to the delicate silicon detectors. The PXD group has extensive plans for measurements during the commissioning period, which can only be briefly summarize here:

- Temperature and humidity sensors: The proper environmental conditions inside the silicon detectors' chamber are vital to ensure the safe operation of the sensors. During the commissioning detector operation, the chamber will be instrumented with several temperature and humidity sensors, complemented with Bragg fibers for a double cross check. These small devices will be attached directly onto the beam pipe, the PXD cooling blocks, and on the inner and outer surfaces of the thermal enclosure.

- Accumulated doses and instantaneous rates: To complement the PIN diodes from the US institutes, the PXD group will install radFETs and single channel diamond detectors, shown in Figure 7. The diamond detectors can be used both for direct measurements and for calibration of the other detectors. Although the final placement of these devices is not decided yet, the radFETs have to be positioned close to the interaction point to measure the doses that the innermost PXD-layer will receive.

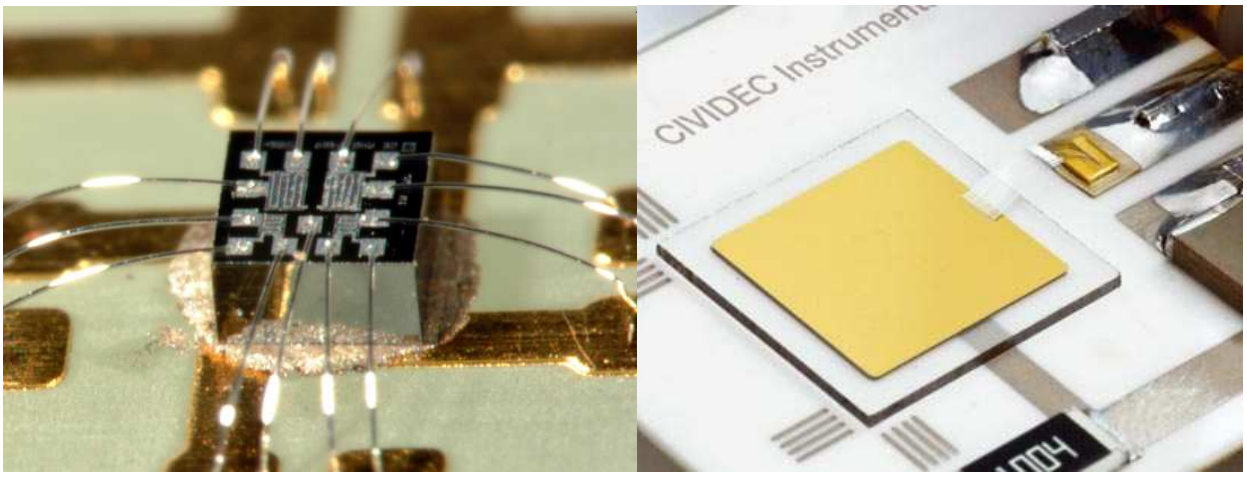

Figure 7: *Left: radFET glued onto a PCB. The wire bonds provide perspective on the detector size. Right: Single channel CVD diamond. The radiation hardness of the diamond detectors makes them very useful for measurements in harsh environments.*

This can be achieved due to the small size of the device combined with thin readout wires. The radFETs, depending on the oxide thickness and operation parameters, could withstand up to a few Mrad without degradation.

The single channel diamonds are bigger devices (of order cm^2) and should stay away of the interaction point due to the lack of space. These devices are operated very close to the interaction point in the LHC experiments, so radiation damage is not an issue at the expected BEAST II doses. A 6-mm thick cable is needed to bias and read the detector.

Diamond sensors will also be used as fast detectors in a beam loss abort system. The proposed layout comprises 4 stations in the forward and 4 in the backward regions, close to the beam masks, in the horizontal and vertical directions.

The PXD group will provide manpower for the design, installation, data taking and analysis of the detectors discussed. In addition, the PXD group can do the electron irradiation of the PIN diodes to be provided by the US groups using the ELSA Linac 1 accelerator (Bonn, Germany), with 17 MeV electrons.

- Near field antenna: The PXD group expects also major noise contributions considering the fact that the innermost layer of the pixel detector will be just 2 mm away of the surface of the beam pipe. To explore the noise contribution on the PXD sensors, a near field antenna, designed especially for this purpose, will be installed instead of one DEPFET ladder. In addition, this device can help the SuperKEKB machine group in the commissioning of the accelerator.

- Photon energy spectrum: The photon energy spectrum has to be measured with high resolution (down to a few keV) in order to estimate the synchrotron radiation in the

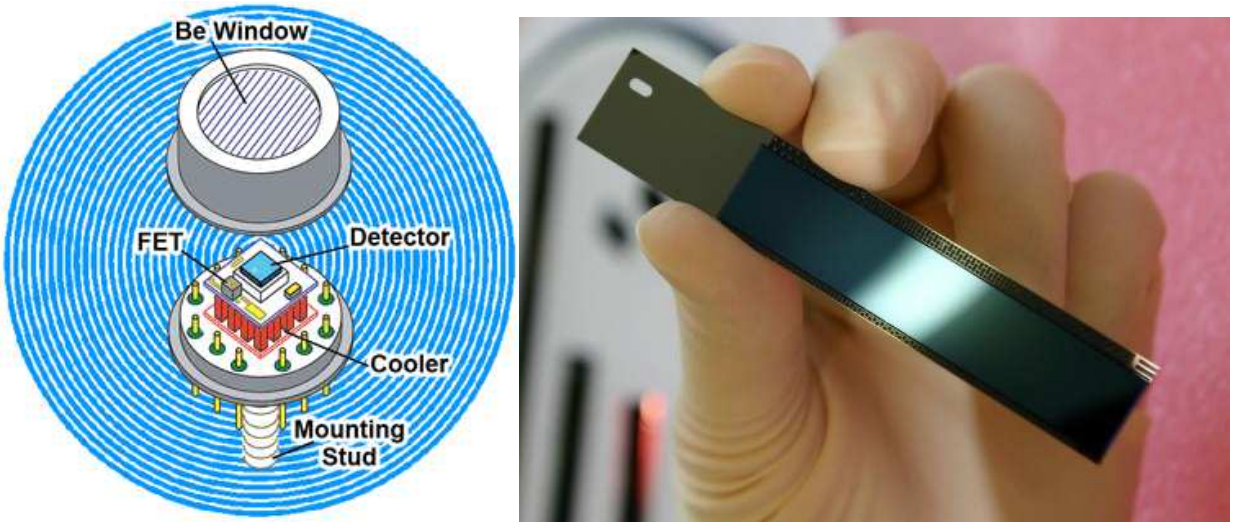

Figure 8: *Left: The photon energy spectrum has to be determined with high accuracy. One of the proposals is the use of silicon drift detectors. Right: Half DEPFET ladder after being cut from the wafer. One full ladder will be obtained by gluing two half pieces as the one shown here.*

detector, and to study the radiation damage to DEPFET sensors in this range. The final device has not been decided on yet, but a small silicon drift detector seems suitable for this purpose. The detector has to be as close as possible to the final DEPFET sensor location, in order to measure the real photon spectrum the PXD will see. The PXD group will contribute with manpower for the installation, data taking and data analysis.

- Once the radiation levels have been determined to be sufficiently low, two DEPFET ladders will be installed in their nominal Belle II positions, to exercise the assembly and operation procedures of the final PXD. The ladders have to be operated under final conditions, and the full services that will later be used for the real PXD have to be ready and operational. These services include data transmission, DAQ, power supplies, the CO_2 cooling plant, the cooling and support structures around the beam pipe, capillaries for air cooling and the thermal enclosure for the SVD and PXD. The PXD group will install the detector, and operate and analyze the data.

1.1.10 Commissioning Detector Luminosity Monitoring Device

Introduction

Members from the National Taiwan University High Energy Physics Group (NTUHEP), including YuTan Chen, GuanBo Lin, and FaHui Lin, led by Professor Min-Zu Wang and Dr. Jing-Ge Shiu, will contribute to the luminosity monitoring device for BEAST2. FaHui Lin and Yutan Chen will install this device in the summer of 2014. Some other members in the

NTUHEP will operate it after that.
The luminosity monitor can provide: (1) luminosity information using coincidence signals from the back-to-back feature of candidate Bhabha events, and (2) background intensity with accumulated charges as a function of time.

Detecting System

This monitor consists of 8 sets of BGO (Bismuth Germanate) scintillation crystals fixed around the interaction point. A full ring version of this device has been used at Belle for the luminosity monitoring of KEK-B, and has been proved to be radiation hard (up to an accumulated dosage of 100 Mrad). The scintillation lights of each BGO crystal will be imaged through an array of optical fibers onto photomultiplier tubes in the readout system.
There are different commissioning scenarios for BEAST2. In T0 and T1 scenarios, the BGO luminosity monitor is not very useful since there is no collisions. However, this device can function as a background monitor (with background current measurement circuits) and can be located at places other than the VXD volume if necessary. In T2 scenario (no SVD nor PXD installed), the BGO luminosity monitor is installed inside the VXD volume, right near the interaction point. These 8 BGO crystals are mounted on 2 aluminum rings (i.e. 4 crystals on one ring), which are fixed to the inner tube in VXD volume. The 4 forward crystals are located at the line with an angle of 11.5° by the symmetric axis, while other 4 backward crystals are located with an angle of 20° by the symmetric axis. (Figure 1 and Figure 2).

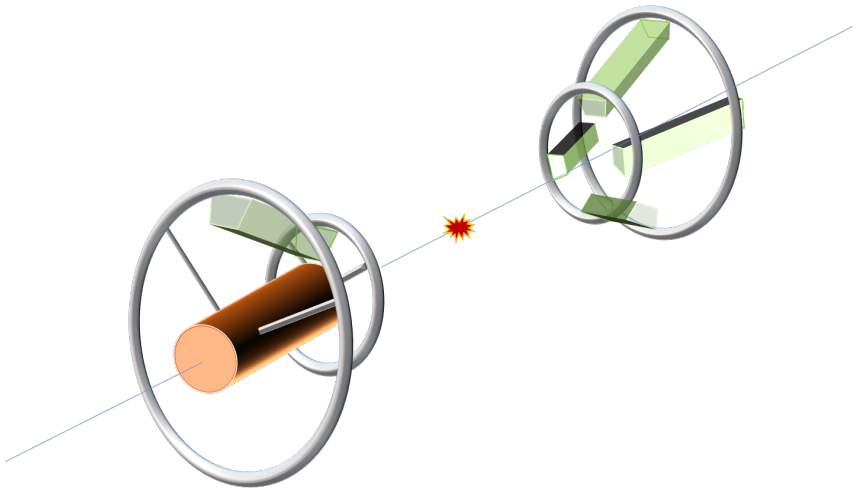

Figure 9: A 3-D conceptual drawing for BGO crystals (green) mounted on the aluminum rings (metallic) near the interaction point inside the VXD volume. The brown cylinder shows the inner tube inside VXD volume where the rings can be fixed to with screws and support timbers.

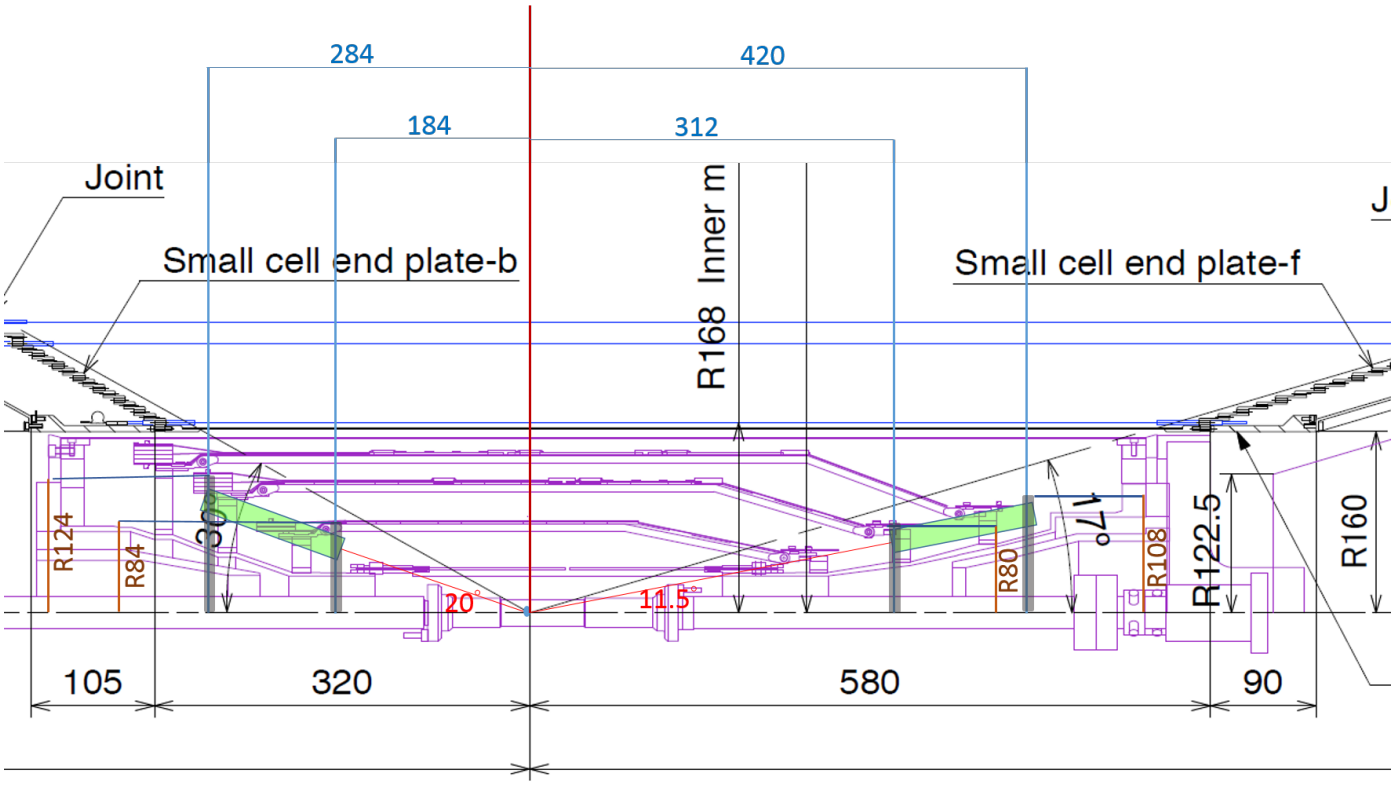

Figure 10: Sub-detector installation blueprint (partial), focusing on the VXD, showing locations of crystals (green) and aluminum rings (gray).

Readout System

We use one MAPMT (multi-anode photomultiplier tube) to receive scintillation lights from BGO crystals. The MAPMT needs $900V$ high voltage and we hope that KEK can provide the HV power supply. There are 8 channels for 8 BGO crystals respectively. Between the crystals and the MAPMT, there are 8 optical fibers, one for each crystal. The fiber array should be about 25 m long. The fibers are put into a soft black hose (also about 25 m long) with a diameter of $\sim$ 1 cm. The required length is to connect the crystal in VXD volume to the MAPMT at the readout system zone. The space needed in the readout system zone should be about 1 m^3 .

The output signals from the MAPMT are charges. After the front-end circuit, the signals become logic signals and digitized charge information. The signal frequency should be kept under 100 Hz with proper threshold settings. The characteristic time or decay time for BGO scintillation is about 300 ns.

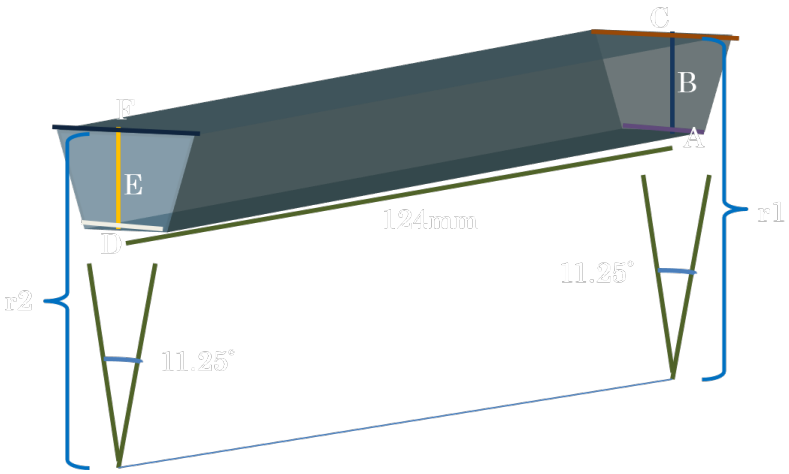

Figure 11: Dimensions of a single BGO crystal.

type	A	B	C	D	E	F	r1	r2
B5 (mm)	22.938	12.280	25.356	30.828	19.616	34.692	130.48	177.87

The 8 logic signals will go through a logic circuit (implemented with FPGA, as shown in Figure 4) to obtain the coincident signals via the back-to-back feature of Bhabha event. After subtracting the signals from random coincidence, the signal rate gives the luminosity information.

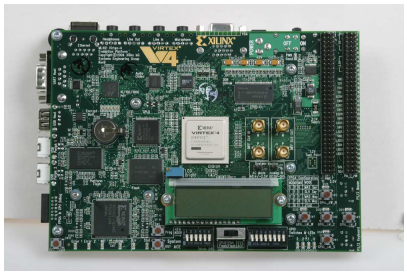

Figure 12: The Xilinx vertex V4 FPGA board

The first version of the readout circuit will be produced in summer 2013, and the final version will be produced in the end of 2013.

Simulation

The simulation task, using GEANT4, is underway in order to get the conversion factor between the rate of triggered events and the instant luminosity. At this stage, the particlegun

Figure 13: Back-to-back signal Bhabha candidate event Logic: (B1 and F3) or (B2 and F4) or (B3 and F1) or (B4 and F2)

generator is used. We impose an energy cutoff at 0.5 GeV to get rid of background events, which is reasonable from simulation results. This energy cutoff corresponds to the threshold of input signals. From calculation of Bhabha scattering, the luminosity required for one particle detected per second is estimated to be about 10^{30} cm^{-2} s^{-1}.

System Test
There is a plan to check the device response before its installation at KEK. The expected time should be around the spring of 2014. The NTUHEP members will use a radiation testing facility (with a 10^4 Curie Co-60 source) in northern Taiwan to get the conversion factor between the accumulated charge and the received radiation dose. It will be important to have some ideas about the effect of radiation damage or annealing behavior of this monitor in the same test.

1.1.11 Commissioning Detector micro-TPCs

In order to monitor and study neutrons, we will install eight gas-filled micro-TPC detectors. Fast neutrons produce heavily ionizing nuclear recoil via elastic scattering in the gas volume. We will measure the ionization trails produced by these recoils in 3D, by employing a high-resolution TPC charge readout, based on gas electron multipliers (GEMs) and pixel electronics [1]. This makes it possible to tag fast (MeV-scale) neutrons, and to measure both their energy and direction, which is not possible with other types of detectors. The neutron measurements will allow us to identify the neutron production points, which can be used to validate and tune the neutron component in the beam background simulation. At high gain settings, such gas TPCs can also be used to reconstruct minimum ionizing particle (MIP) tracks, and (with thin vessel walls and appropriate positioning) to obtain x-ray spectra in

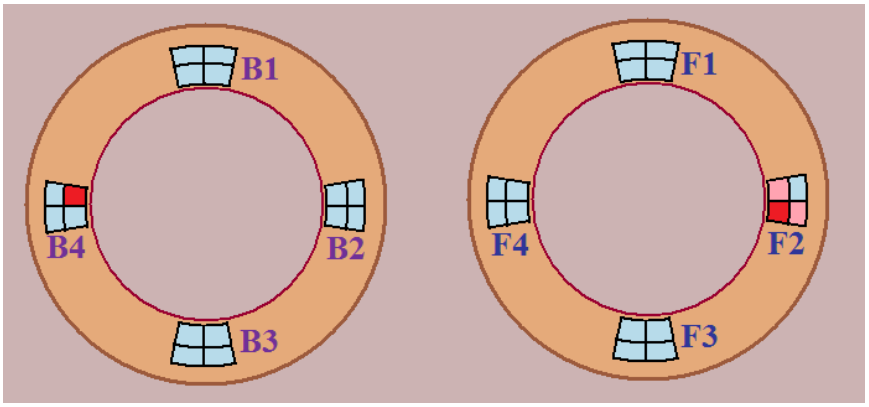

Figure 14: Not Back-to-back signal background event Logic: (B1 and F1) or (B1 and F2) or (B1 and F4) or . . . or (B4 and F4)

	Rate in backward TPCs (MHz)	Rate in forward TPCs (MHz)
Coulomb HER	0.00	0.00
Coulomb LER	0.05	0.09
Radiative Bhabha HER	0.45	3.55
Radiative Bhabha LER	3.45	0.35
Touschek HER	0.05	0.15
Touschek LER	0.55	1.15

Table 2: *Predicted rate of neutrons traversing the backward and forward micro-TPC arrays, at design luminosity.*

the keV range, which would be sensitive to synchrotron light (SR) backgrounds. In that case, energy deposits from MIPs, x-rays, and neutron recoils can be distinguished via the specific ionization (dE/dx) and ionization pattern measured. Since we already plan to use diodes for measuring x-rays, and expect to install a drift chamber prototype for tracks, we will optimize the TPCs for neutrons, but at the same time it will be good to have some redundancy in our commissioning setup, where the unexpected typically does occur. The micro-TPCs will be radiation hard (up to at least 50-100 Mrad), and capable of high data rates, as they will employ pixel chips developed for the ATLAS experiment at the LHC.

Figure 17 shows the trajectories of neutrons that deposit energy in the calorimeter, for two types of beam background. The majority of neutrons are generated near the QCS magnets, but the detailed distributions differ by background type. To monitor these neutrons in detail, we will position the micro-TPCs between both the forward and backward QCS magnets and the ECL calorimeter, i.e. at a radius of 70 cm from the beamline, positioned at z=1 m and

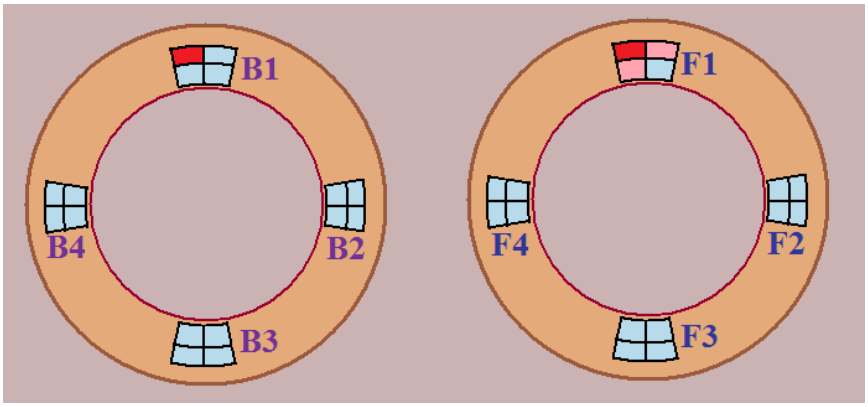

Figure 15: Geometry of BGO Luminosity Monitor, made up of 8 BGO crystals, plotted with GEANT4 in BASF2

z=-1 m along the beams. There will be four TPCs at each z position, mounted 90 degrees apart in azimuthal angle, so that we can measure the ϕ-distribution of the neutrons, which is not flat (see e.g. Fig. 6, and similar plots in the KLM system chapter). Each TPC will have an active volume of 5 cm $\times$ 5 cm $\times$ 20 cm. The longest dimension is the direction of the TPC drift field, which will be parallel to the Belle II solenoid magnetic field, to minimize diffusion of drift charge. 13 cm^2 of the 5 $\times$ 5 cm readout plane would be instrumented with pixels, the rest of the area will be used for gain calibration of the TPCs. The radial positioning of the TPCs will depend on the amount of neutron shielding to be used in the commissioning detector, and may vary between the different stages of commissioning. If no neutron shielding is used, all TPCs can stay at r=70 cm for the entire commissioning period, so that they are mechanically independent from the shielding and other monitors. If we decide to install as much as 10 cm of polyethylene during vacuum scrubbing, this would greatly reduce the neutron rate, and wash out the directional information at r=70 cm. In that scenario we would mount half of the forward and backward TPCs between the high-Z and polyethylene during this period, with the center of the TPC at r=35 cm. That would allow us to simultaneously study the (unshielded) production of neutrons, while monitoring the (shielded) rate of neutrons incident onto the ECL.

Figure 18 shows the polar angle distributions of only those neutrons which traverse the TPCs at the nominal position of r=70 cm, for each beam background process. The difference in the angular distributions, combined with the different dependence of each background process on accelerator parameters (beam current, luminosity, beam size, and vacuum pressure), should allow us to distinguish and measure the neutron production from each process during beam commissioning. The rates of neutrons traversing the TPCs are given in table 2, and are very large at design luminosity - of order 100 kHz to MHz. The fraction of neutrons that scatter elastically and lead to a reconstructable recoils in the TPCs, however, is low, of order 0.1%. As a result the expected signal rate in each TPC is of order a kHz at design

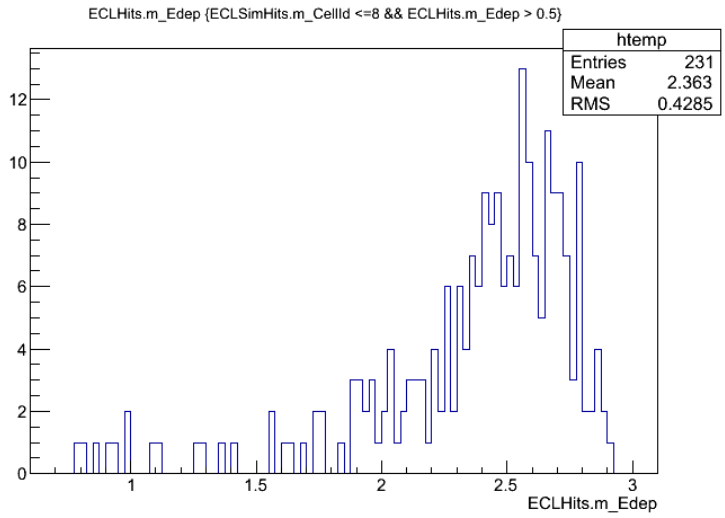

Figure 16: Simulation of 1000 events (e^+, e^-, γ) with energy 4 GeV at $\theta = 10.5°$ to $12.5°$, and full range of ϕ.

luminosity. As discussed above, all backgrounds except those from beam-gas are expected to be much lower during commissioning, while those from beam-gas could be much higher. The pixelated TPC image plane will be read out at 40 or 80 MHz, which is fast enough to separate individual recoils even at the highest possible neutron rates, of order GHz, due to the low probability of elastic scattering. In that scenario we would run in a pre-scale mode, where we only read out and save a fraction of the events.

The micro-TPCs with GEMs and pixels are innovative, but low risk, as readily available components will be employed: standard GEMs available from CERN, the ATLAS FE-I4 pixel chip (available from LBNL), and DAQ electronics available from SLAC. The combined operation of GEMs and ATLAS pixels was previously demonstrated with a 1 cm^3 prototype at LBNL, by a team including Hawaii faculty member Vahsen. The LBNL prototype measured charged tracks with excellent (< 100 μm) point resolution, and obtained FE-55 x-ray spectra with good (about 20% FWHM) energy resolution [1]. The Hawaii group recently constructed a similar micro-TPC prototype, which is currently being commissioned. First results from Hawaii, shown in Fig. 19, also indicate excellent detector performance, and the group is currently demonstrating neutron detection. Neutrons can be detected in gas TPCs by reconstructing the nuclear recoils resulting from elastic scattering of the neutrons with the nuclei in the target gas. Figure 20 shows a simulation of 1-MeV hydrogen nuclei recoiling in atmospheric-pressure isobutane gas. The ionization trails from such neutron-induced recoils are of similar length as the cosmic track shown in Fig. 19, but the expected amount of ionization is of order hundred times greater for nuclear recoils, and hence much easier to detect. For the commissioning detector, we expect to use a helium-based gas mixture.

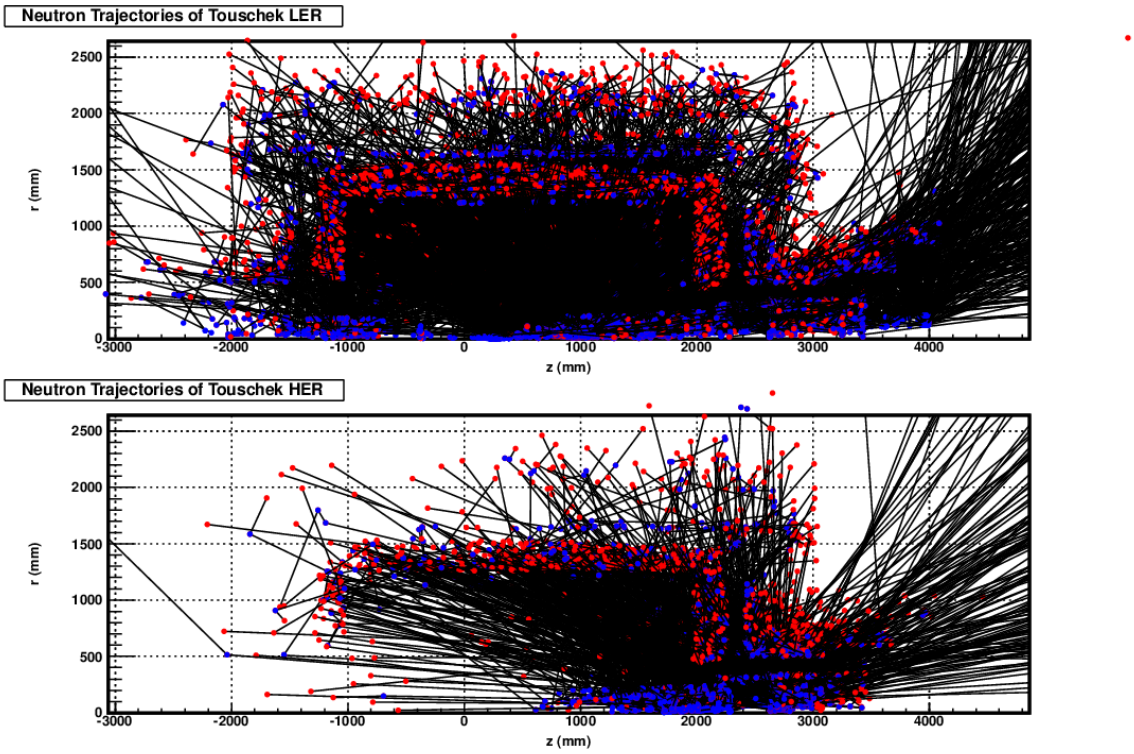

Figure 17: *GEANT production points (blue), GEANT decay points (red), and trajectories (black) of neutrons that deposit energy in the calorimeter, for Touschek backgrounds originating from the low energy ring (upper) and high energy ring (lower).*

As the University of Hawaii group is already developing TPCs for fast neutron detection [4][5], relatively modest resources are needed to adapt them to the commissioning detector. Before production of the final micro-TPCs for the Belle II commissioning detector can begin, they will perform a final round of prototype optimizations and demonstrations. The group will design a new gas vessel, and slightly modify the layout of the readout electronics so that they are compatible with the micro-TPC geometry. The final prototype demonstration will include detailed neutron source measurements, as neutron detection (through the tracking of nuclear recoils from elastic neutron/gas-nucleus scattering) has not been explicitly demonstrated with the specific TPC readout technology used, though it has been demonstrated with very similar TPCs [3]. A collimated neutron source for these tests has already been constructed, and first neutron measurements are ongoing. The final demonstration should use the new ATLAS-FE-I4 pixel chip. Previous measurements at LBNL and Hawaii used the older ATLAS-FE-I3 pixel chip, but FE-I4 has an active area of 3.36 cm^2, almost three times that of FE-I3. This has the advantage that only four readout chips will be needed to instrument the 12 cm^2 readout plane of each micro-TPC.

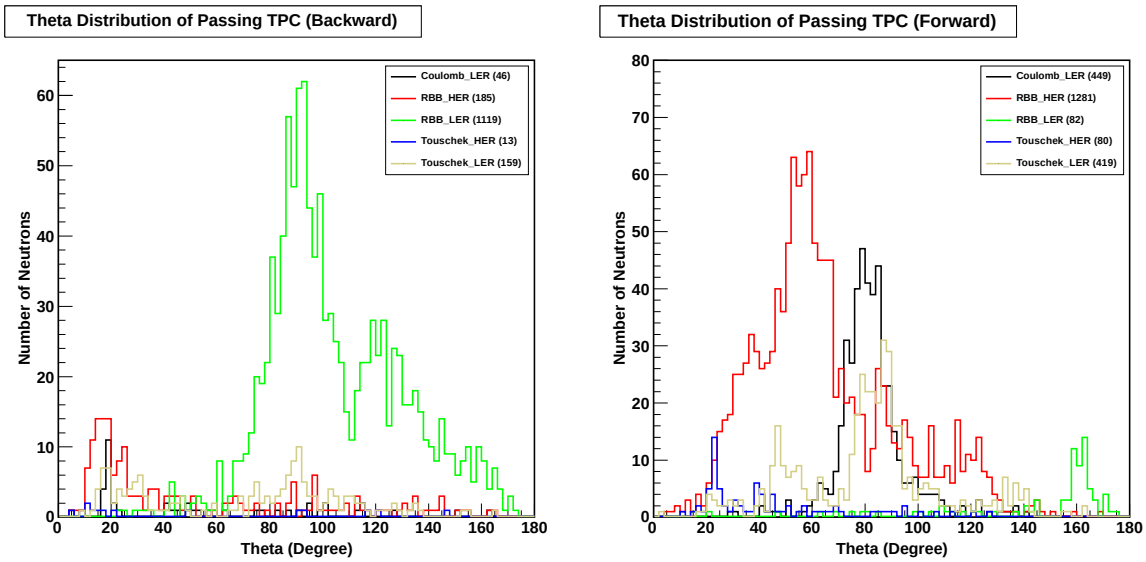

Figure 18: *Polar angle of neutrons that pass through the backward (left) and forward (right) array of micro-TPCs. The angle plotted is the polar angle of the incoming neutron direction, as seen by each micro-TPC.*

References

[1] T. Kim, M. Freytsis, J. Button-Shafer, J. Kadyk, S. E. Vahsen and W. A. Wenzel, "Readout Of TPC Tracking Chambers With GEMs And Pixel Chip", Nucl. Instrum. Meth. **A589** (2008), 173-184

[2] R. Cizeron, A. Durand, T.L. Geld, V. Lepeltier, B. Meadows, Michael T. Ronan, S. Sen, A. Valassi, G. Wormser, "A Mini - TPC for SLAC B factory commissioning", Nucl. Instrum. Meth. **A419** (1998), 525-531

[3] K. Miuchi et al., "Performance of a micro-TPC for a time-resolved neutron PSD", Nucl. Instrum. Meth. **A517** (2003), 219-225

[4] J. Yamaoka, H. Feng, M. Garcia-Sciveres, I. Jaegle, J. Kadyk, Y. Nguyen, M. Rosen, S. Ross, T. Thorpe, S. Vahsen, "Application of Time Projection Chambers with GEMs and Pixels to WIMP Searches and Fast Neutron Detection", TIPP2011, submitted to Elsevier Physics Procedia (2011)

[5] S. E. Vahsen, H. Feng, M. Garcia-Sciveres, I. Jaegle, J. Kadyk, Y. Nguyen, M. Rosen, S. Ross, T. Thorpe, J. Yamaoka,"The Directional Dark Matter Detector", arXiv:1110.3401v1 (2011)

[6] Belle II Technical Design Report, `http://xxx.lanl.gov/ abs/1011.0352`

[7] A. Piwinski, "The touschek effect in strong focusing storage rings", Mar 1999.

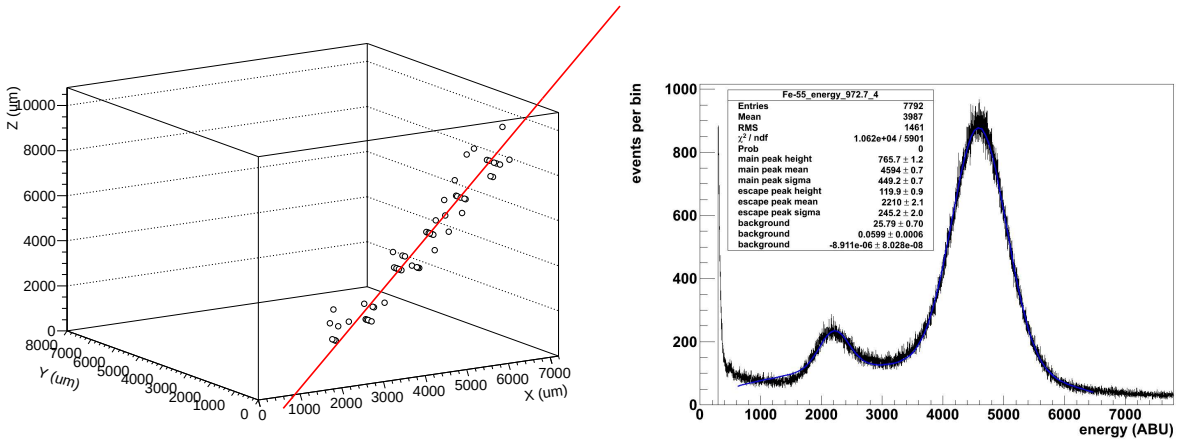

Figure 19: *Example of cosmic ray track (left) and FE-55 x-ray spectrum (right) recorded with micro-TPC prototype at the University of Hawaii.*

[8] H. Nakayama et al, "Small-Beta Collimation at SuperKEKB to Stop Beam-Gas Scattered Particles and to Avoid Transverse Mode Coupling Instability", IPAC-2012-TUOBC02.

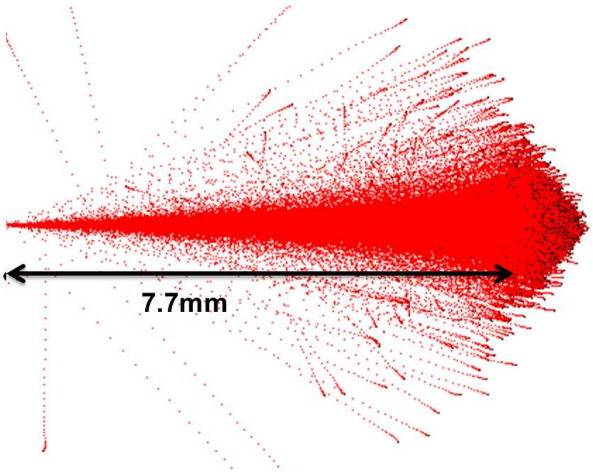

Figure 20: *Simulation of ionization deposited by 1-MeV Hydrogen nuclei in* C_4H_{10} *gas at 1 atmosphere.* 10^5 *recoils with identical start position and velocity have been superimposed for visibility.*

A Appendix: SuperKEKB Commissioning Detector

This appendix contains supplementary information relevant to the commissioning detector, such as results from simulation studies, which guided the design of the commissioning detector in general and TPC system in particular, a more detailed discussion of the US contribution, and a description of contributions from non-US institutions.

B micro-BEAST-TPCs simulation

In this section, Monte Carlo simulations studies of the micro-BEAST-TPCs are described. These studies were performed in order to design and optimize the micro-BEAST-TPCs to be able to distinguish the different beam-induced backgrounds (Touschek, Radiative Bhabha and Coulomb) by measuring the angular distributions of the nuclear recoils procured when neutrons scatter elastically off the nuclei of the gas-target.

These section is divided into three parts: the **simulation framework** is introduced, the **design optimization** and the neutron **detection efficiency** are presented.

B.1 Simulation framework

Our Monte Carlo study of micro-BEAST-TPC performance is based on two detector simulators: BASF2 and CYGNUS (our TPC-simulator). BASF2 and CYGNUS are both a full detector simulator based on GEANT4 but also on a Fast Monte Carlo or Full simulation for CYGNUS. Our Fast Monte Carlo is based on MAGBOLTZ. Our Full simulation is based on SRIM and GARFIELD. At the moment, both simulators are separated but we are currently working in combining the GEANT4 part of CYGNUS into BASF2.

B.1.1 Simulation strategy

A two steps simulation strategy is adopted to enhance the recoil number due to the low neutron cross section and also because GEANT4 is not simulating the electrons drift under the influence of an electric field.

- first step: BASF2 simulation of the different beam-induced backgrounds. This step is used to determine the types, origins, energy and angular distributions of the particles passing through the micro-BEAST-TPCs ie the beam-induced particles background profiles.
- second step: beam-induced particles background profiles served as an event generator for CYGNUS

B.1.2 BASF2

BASF2 tracks particles due to the beam-induced background from the interaction points through various Belle2 detector components, taking into account their various interactions with detector materials. There are three types of beam-induced background: Radiative Bhabha (RBB), Coulomb and Touschek. These beam-induced backgrounds are producing mostly electromagnetic particles and neutrons. We are planning to produce beam-induced background simulation corresponding to phase 2 stage. Phase 1 stage can not be used to test

the beam-induced background simulation at the designed luminosity so there is no interest to simulate this stage. All our studies are based on the 5th compaign of beam-induced background simulation produced by Nakayama-San at the designed luminosity and with the full Belle2 setup. The luminosity at the end of phase 2 should be 100 smaller than the one at designed luminosity. All rates originating from RBB, Touschek and Coulomb bacground presented below have been scaled by a factor 1/100. It should be noted only RBB background is scaling with luminosity. Touschek and Coulomb backgrounds are not scaling with the luminosity and only require one beam. Touschek background is scaling with the particles density per beam bunch. Coulomb or beam-gas bakcground is scaling with the Pressure. So in principal in phase 2, the Touschek and Coulomb background rates can be increased by the accelerator people by increasing respectively the beam bunch density and the pressure in the beam pipe.

B.1.3 TPC-simulator (CYGNUS)

The TPC-simulator aka CYGNUS is done in two steps:

- first step: beam-induced particles background profiles served as an event generator for the GEANT4 part of CYGNUS.
- second step: Fast Monte Carlo for
  - electron drift parameterization (using v_{drift}, D_l and D_t)
  - GEMs or avalanche-charge parameterization
  - digitization into pixel hit

Figure B.1.3 shows a flow chart of CYGNUS. There is the possibility to use a full simulation for the electron drift and also to use SRIM transport model instead of SRIM-like GEANT4 transport model.

Figure B.1.3-left shows a G4 drawing of a single micro-BEAST-TPC and a G4 drawing of eight micro-BEAST- TPCs located in the dock space (Figure B.1.3-right).

B.2 Design optimization

B.2.1 TPC position

At this stage, we can not determine the optimum position for the T1 phase. For the phase 2 phase, the TPCs will be located in the dock space. Figures B.2.1 and B.2.1 represent two section views: a top view and r-phi views for the backward and forward dock spaces. The rectangular red boxes show the possible TPC positions. Figure B.2.1 gives also the TPC numbering. The TPCs can be located at different z positions in the backward and forward dock spaces: -210 $\leq$ z $\leq$ -105 cm and 155 $\leq$ z $\leq$ 212 cm respectively.

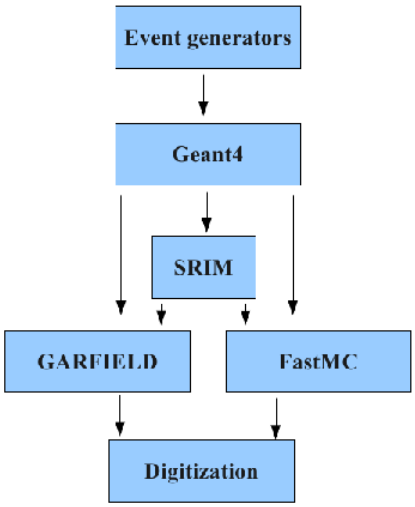

Figure 21: Flow chart showing the simulation steps.

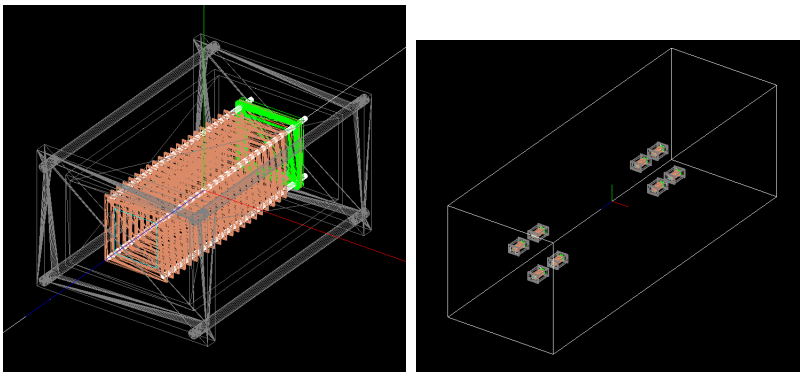

Figure 22: Left: G4 drawing of a single micro-BEAST-TPC. Right: G4 drawing of eight micro-BEAST-TPCs located in the dock space.

Table 3: TPC positions in the dock spaces at phase 2.

TPC #	1	2	3	4	5	6	7	8
r [cm]	37	37	37	37	32	32	32	32
z [cm]	-122	-122	-122	-122	190	190	190	190
ϕ [^{o}]	-90	0	90	180	-90	0	90	180

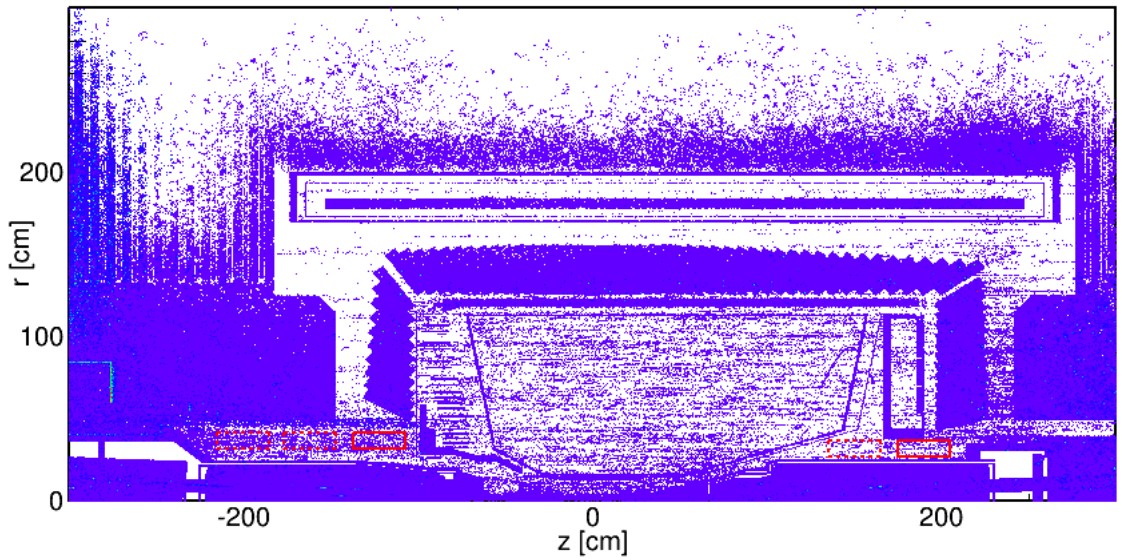

Figure 23: Top view. Distribution for the particle decay points in the radial plane r = $\sqrt{x^2 + y^2}$ versus z-axis.

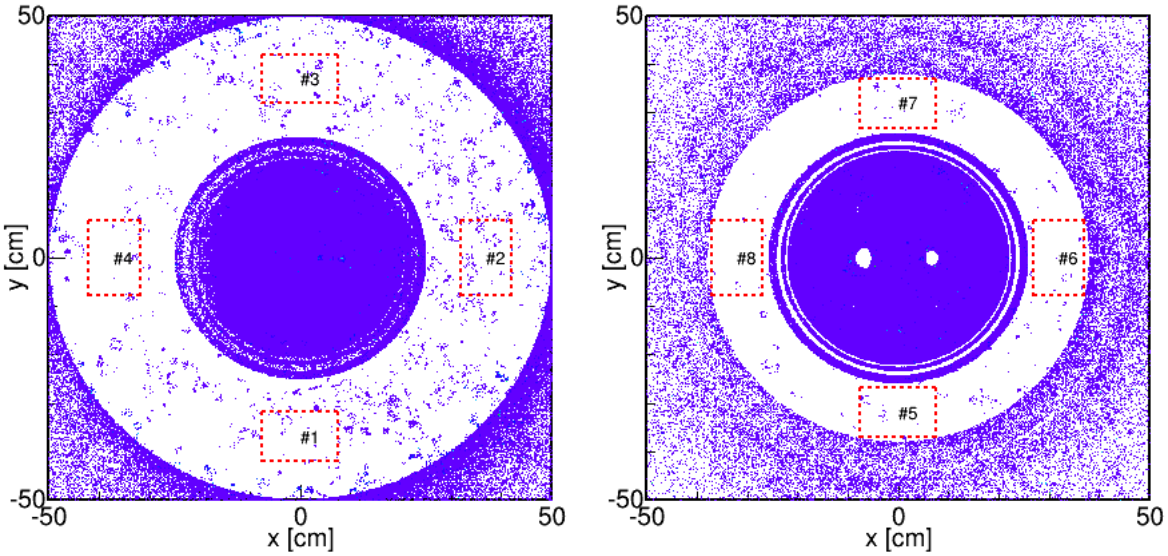

Figure 24: R-phi view. Distribution for the particle decay points in the plane perpendicular to the z-axis. Left: for -210 $\leq$ z $\leq$ -105 cm ie backward dock space. Right: for 155 $\leq$ z $\leq$ 212 cm ie forward dock space.

Table 4: Iso-butane optimized drift velocity and field.

chip	time resolution [ns]	pixel size [μm]	v_{drift} [μm/ns]	E [kV/cm]	D_t [$\mu m/\sqrt{cm}$]
FE-I3	25	400	16	0.5	130.5
FE-I4	25	250	10	0.3	148

The rates at phase 2 for the different beam-induced backgrounds are shown in Figure B.2.1 at the locations corresponding to the full red line box of Figure B.2.1-top-left and Table 3. Figure B.2.1(-top-right and bottom) show also the rates at alternative locations corresponding to the dashed red line boxes of Figure B.2.1-top-right and -bottom. The neutron rates amount of 10 % of lower to the total rate. The rates at phase 2 phase will be 100 smaller than the rates at designed luminosity. The rates of reconstructible events that the TPCs can measure will be at least 1000 smaller. So all together at phase 2 phase should be around few 10's Hz at best.

The neutron rates summed for the backward and forward TPCs traversing the TPCs was estimated at phase 2 as function of the neutron kinetic energy, neutron polar and azimuthal angles as seen in Figures B.2.1-top-row and **??**-top-row and corresponding to the positions of Table 3. The (proton) recoil rates expected was calculated by a Fast Monte Carlo simulation using the two-body kinematic and considering a neutron detection efficiency of 0.1 % in average.

The dominant beam-induced background are RBB LER and HER and Touschek LER. As function of z the RBB LER and HER rates are more or less constant, while the Touschek LER is decreasing in the backward dock space for negative z because they are further away from the QCS. Although the rates emanating from the tunnel increased for smaller z (labeled far in Figure B.2.1), the rates will be most likely of the same level than the internal irreducible TPC background.

B.2.2 Gas choice

The gas choice depends of several factors. It should be composed of a light gas-nucleus in order to have a good neutron elastic cross section and also to have recoil with enough energy to produce long enough track that can be detected and still have directionality. In addition, the gas or the gas-mixture should have a drift velocity high enough to clear the chamber volume rapidly but no too high to have a good 3D hit resolution. The drift velocity will be limited in our case by the pixel size 250 μm for the FE-I4 and 400 μm for the FE-I3: v_{drift} x FE-I3/4 time resolution $\leq$ pixel size. For FE-I3: $v_{drift}(E/P) \leq \frac{400\mu m}{25ns} = 16$ μm/ns and for FE-I4: $v_{drift}(E/P) \leq \frac{250\mu m}{25ns} = 10$ μm/ns. Tables 4 and 5 show the maximum values of $v_{drift}(E/P)$ for the lowest D_l at low drift field to keep drift voltage reasonably low and cage field simple for iso-butane and the gas mixture He:CO_2:70:30.

The attachment coefficient should also be low. The gas gain should stable and on the

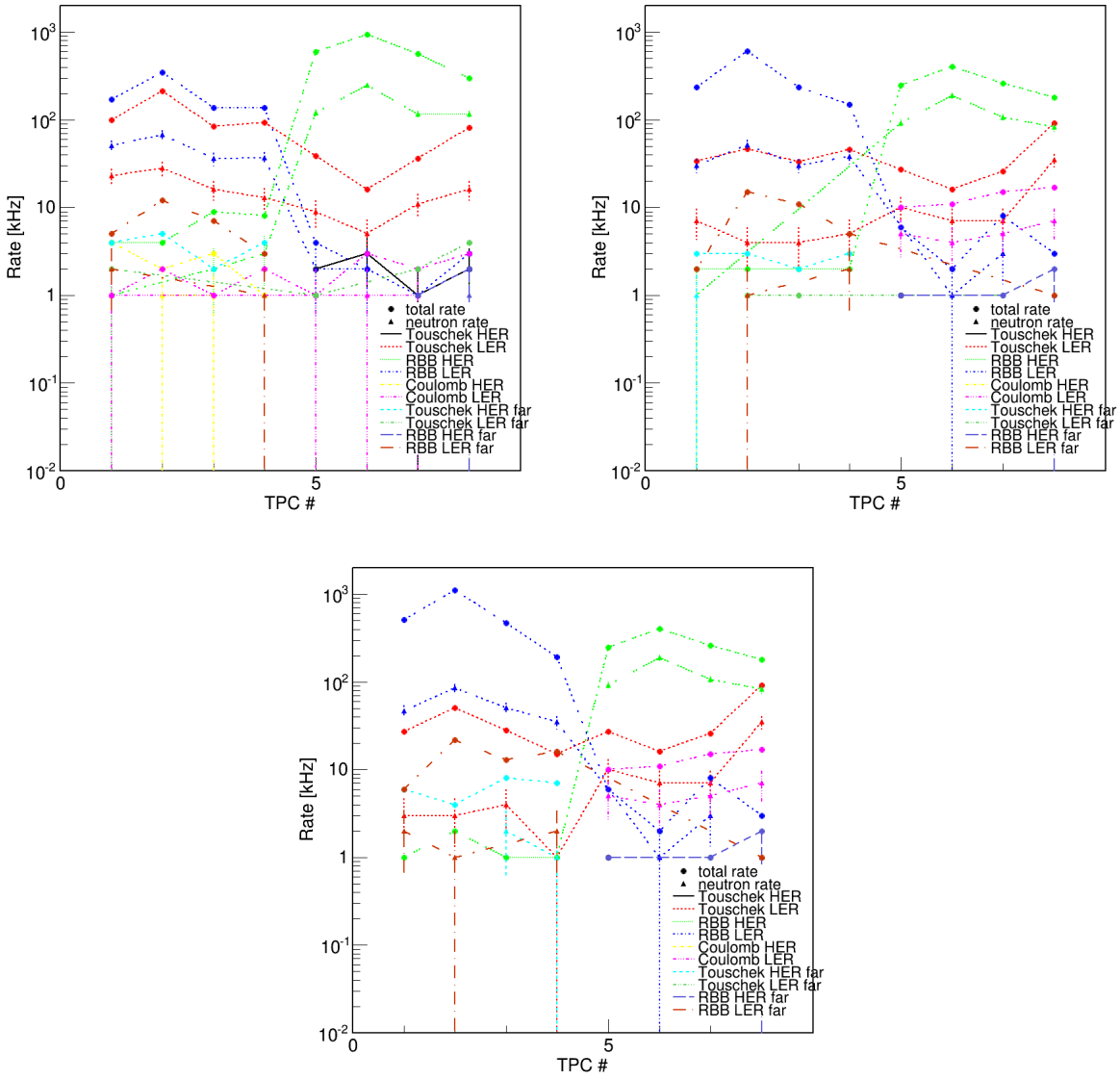

Figure 25: Rates at phase 2 of the different beam-induced backgrounds inside each TPC at different dock space locations. The numbering corresponds to Figure B.2.1. Left top: rate corresponding to the full red line box in Figure B.2.1. Right top and bottom: rates corresponding to the dashed red line boxes in Figure B.2.1. Point symbol total rate. Triangle symbol neutron rate.

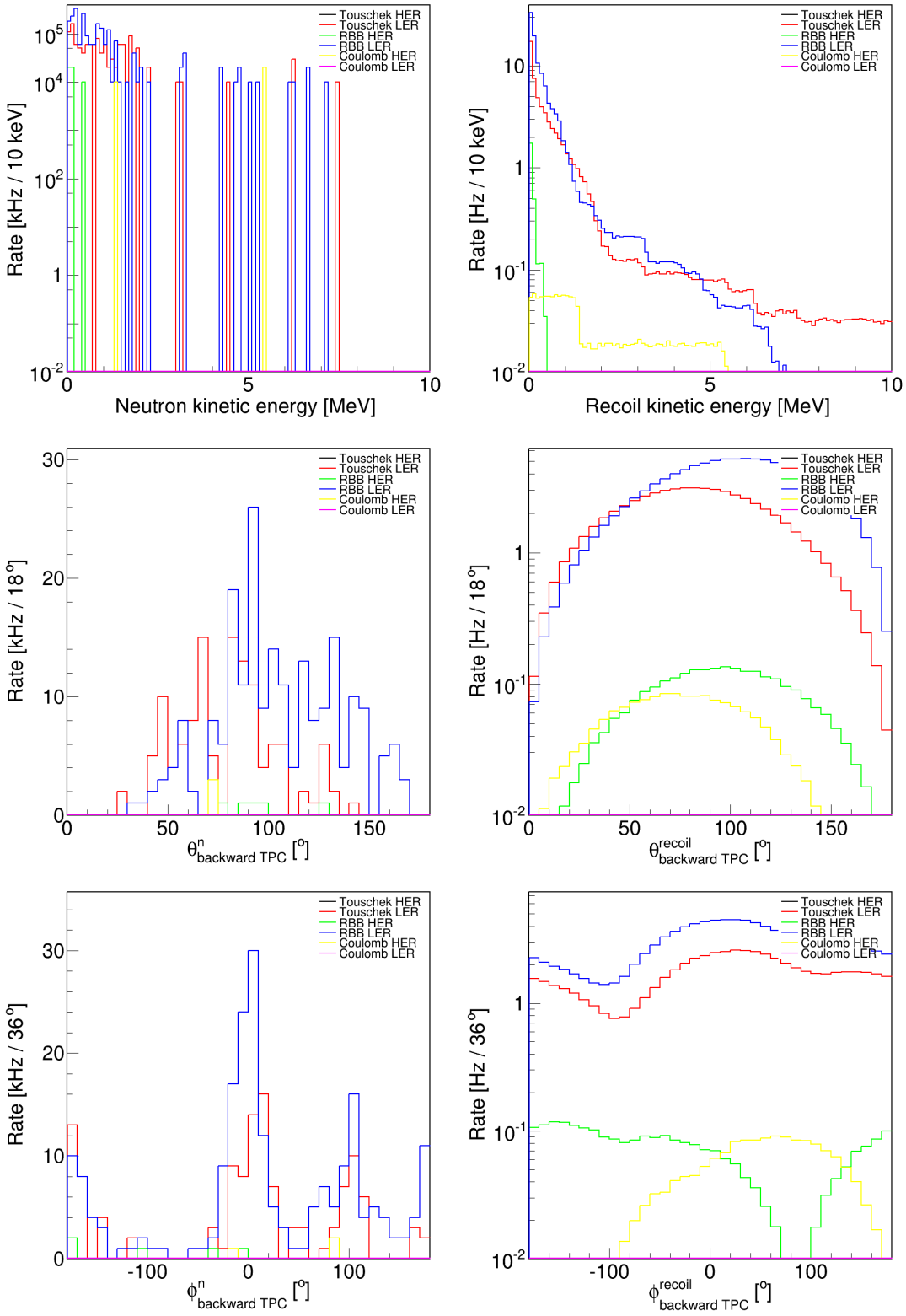

Figure 26: Rates at phase 2 for the beam-induced backgrounds traversing or expected to be measured by the TPCs located in the backward dock-space. Left column: neutron. Right column: proton recoils. Top row: versus kinetic energy. Middle row: versus polar angle. Bottom row: versus azimuthal angle.

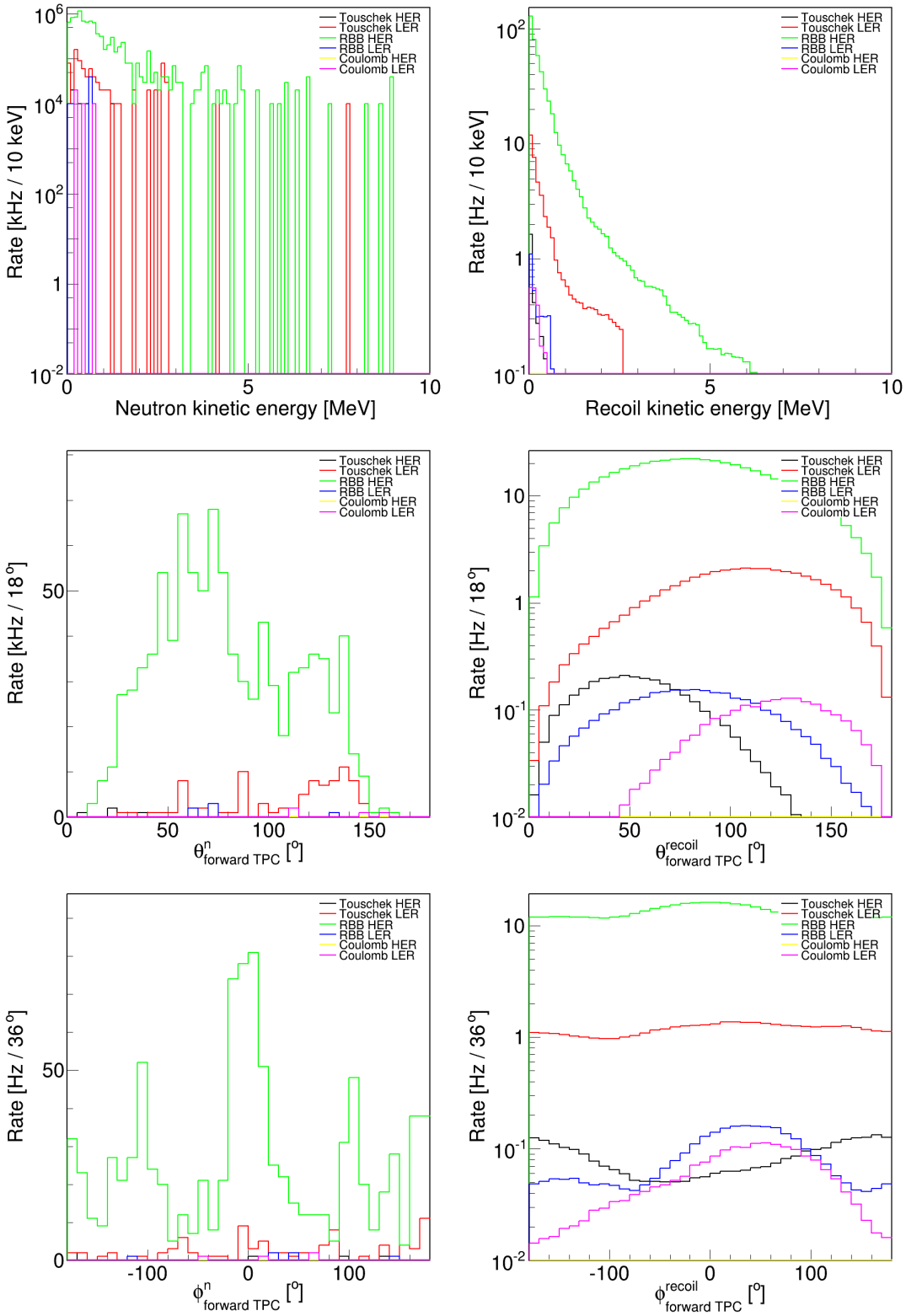

Figure 27: Rates at phase 2 for the beam-induced backgrounds traversing or expected to be measured by the TPCs located in the forward dock-space. Left column: neutron. Right column: proton recoils. Top row: versus kinetic energy. Middle row: versus polar angle. Bottom row: versus azimuthal angle.

Table 5: He:CO_2:70:30 optimized drift velocity and field.

chip	time resolution [ns]	pixel size [μm]	v_{drift} [μm/ns]	E [kV/cm]	D_t [$\mu m/\sqrt{cm}$]
FE-I3	25	400	16	0.84	124.5
FE-I4	25	250	10	0.53	124.3

order of 100 for each GEMs. Several gas and gas mixture: iC_4H_{10} (flammable and explosive), Ar:CO_2, He:CO_2, He:CF_4 and He:CH_4 (flammable, but not explosive), have been investigate with GEANT4 and MAGBOLTZ to determine the neutron probability of interaction per centimeter (Figure B.2.2), the gas parameters respectively and the mixture composition in case of a gas mixture all at 1 atm. Isobutane has the highest neutron cross section 7 to 9 times higher than He:CO_2:70:30.

Figure B.2.2 shows gas parameters: the drift velocity and the diffusion (transverse and longitudinal), for the different gas or gas mixture studied, as function of the electric and pressure (with the pressure at 1 atm) ratio. Figure B.2.2 also illustrates the influence of gases: CH_4, CO_2 and CF_4, which allow depending of the proportion of it compared to Helium to vary the drift velocity for approximately similar diffusions. The evolution of the gas parameters for different proportion of He and CO_2 is shown in Figure B.2.2. The introduction of CO_2 in higher proportion decreases the drift velocity and also lowered the optimal field needed to be applied in the drift region. The influence of the magnetic has also been studies as an illustration, Figure B.2.2 shows the magnetic field influence on He:CO_2:70:30 and iso-butane. In general if the magnetic and the electric field are parallel, the influence of the magnetic field has small effect on gases with small drift velocity. If the magnetic and the electric field are not aligned, the drift velocity and the diffusion parameters expression will be more complicate since for example the diffusion will become tensorial and the drift velocity will have components in all direction.

The gas that offers the best trade off between neutron interaction probability, good gas properties and easy to use is He:CO_2:70:30. Iso-butane is the best gas in general but because its dangerosity make its more challenging but KEK has experience with this type of gas.

B.2.3 Field cage

To minimize the internal background due to natural radioactivity and the neutron probability of interaction with the field cage different width of rectangular rings have been studied using COMSOL. Figure 32 shows the electric field streamlines calculated by COMSOL. Figure B.2.3 shows the radial diffusion as function of the ring width at different transverse positions. The radial distance an electron can drift is below 40 μm ie below the pixel height (50 μm). A mm width can be used for the field cage.

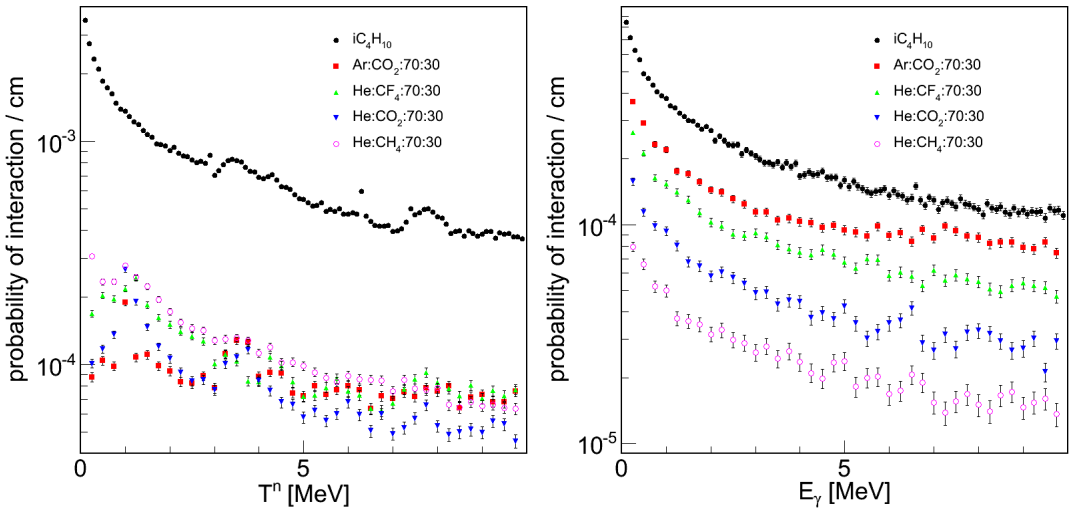

Figure 28: Interaction probability per centimeter as function of kinetic energy for various gas and gas mixtures. Left: neutron. Right: photons.

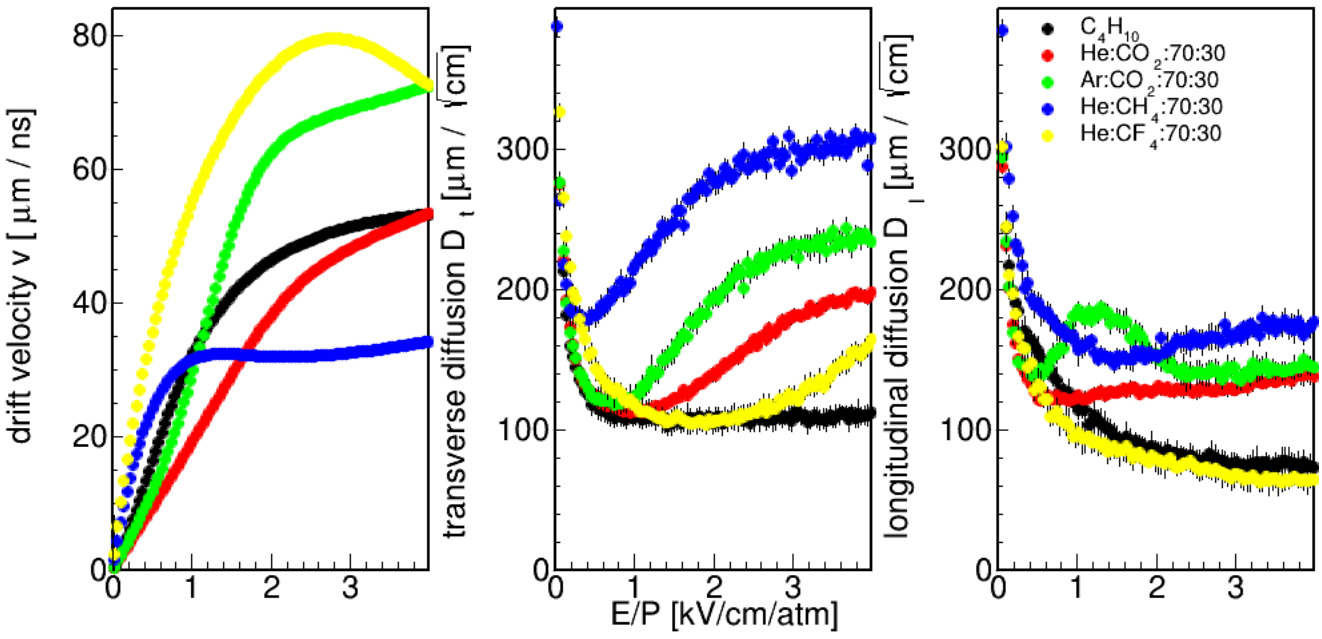

Figure 29: Gas parameters calculated by MAGBOLTZ as function of electric field and pressure (P = 1 atm) ratio for the different gas or gas mixture candidates studied.

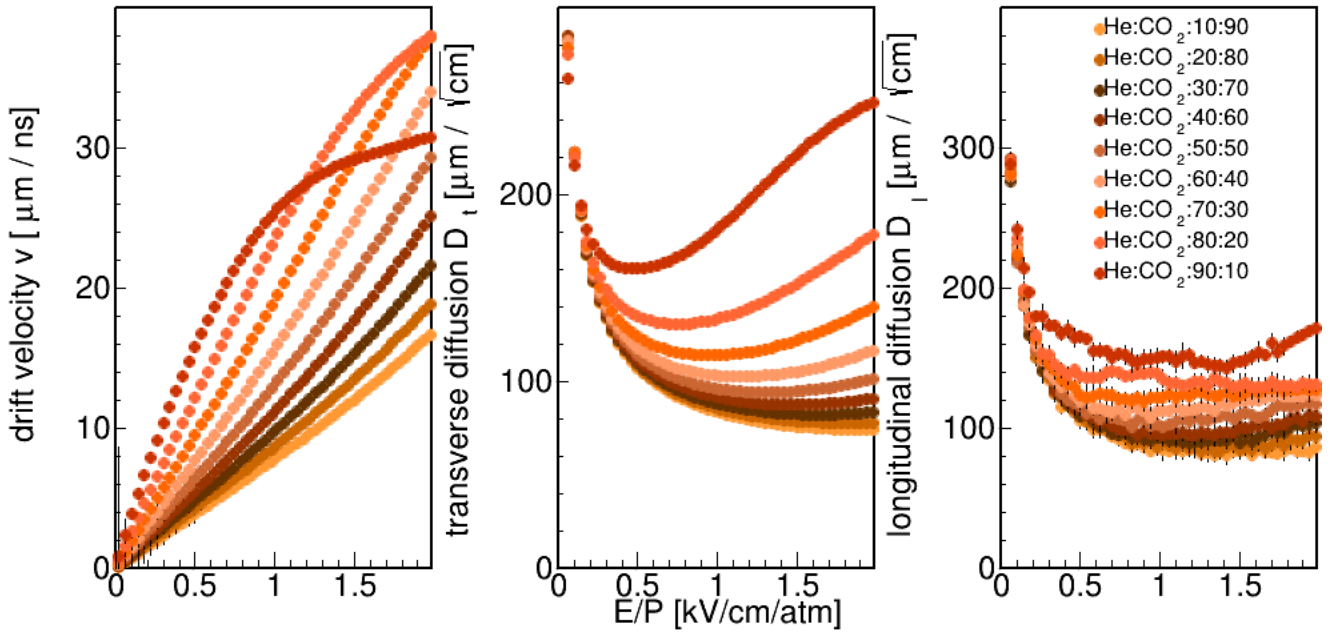

Figure 30: Gas parameters calculated by MAGBOLTZ as function of electric field and pressure (P = 1 atm) ratio for the different percentage of Helium and carbon di-oxygen.

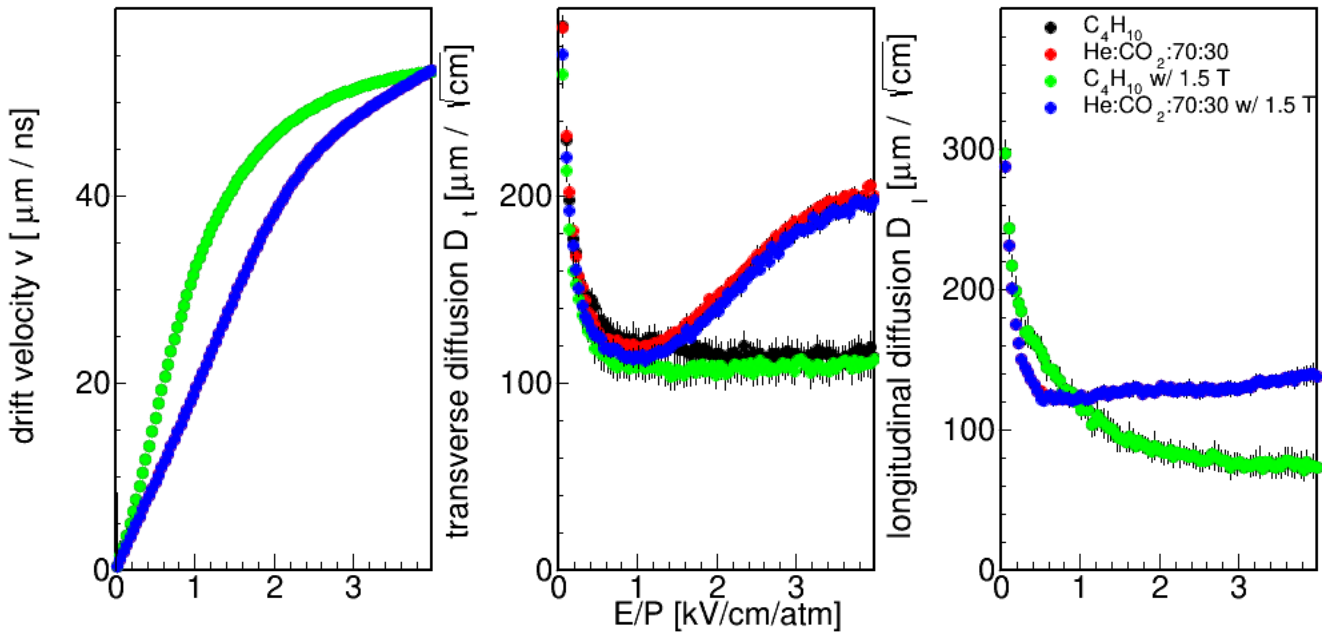

Figure 31: Gas parameters calculated by MAGBOLTZ as function of electric field and pressure (P = 1 atm) ratio for the He:CO_2:70:30 and iso-butane without and with 1.5 T magnetic field.

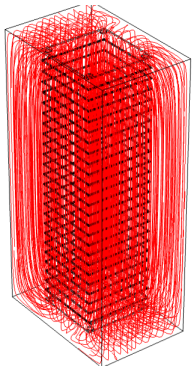

Figure 32: Electric field streamlines calculated by COMSOL.

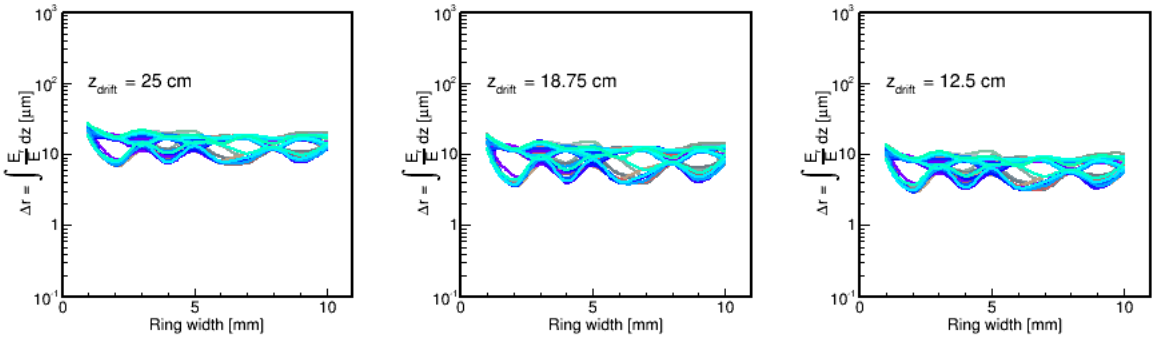

Figure 33: Radial distance an electron drifts from different drift distance to the bottom of the field cage. Left: from top to bottom. Middle: from 18.75 cm to bottom. Right: from 12.5 cm to bottom.

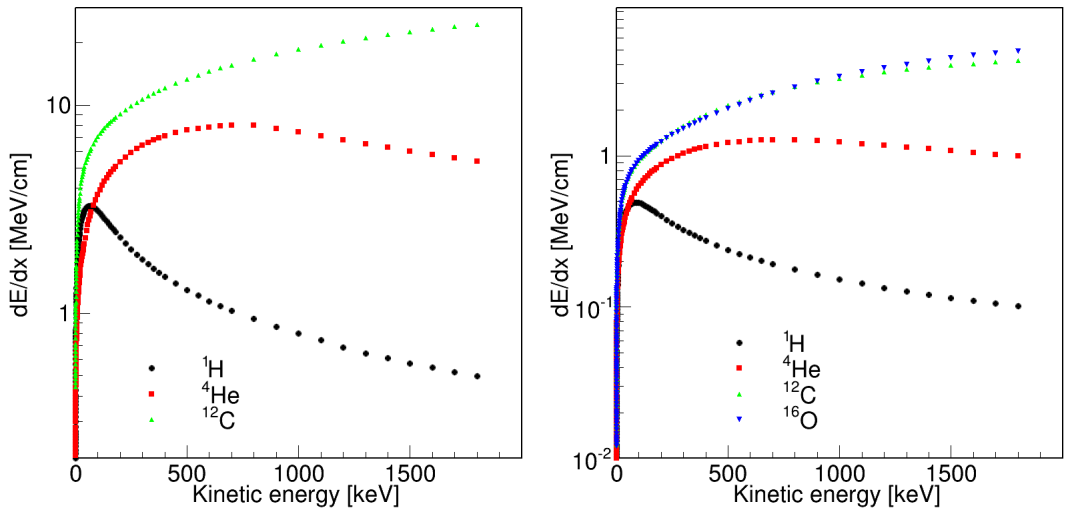

Figure 34: SRIM calculation of electronic energy loss to the gas electron per centimeter versus recoil kinetic energy. Left: Black point H. Red square He, Green triangle C in C_4H_{10} at 1 atm. Right: Black point H. Red square He, Green triangle C and Blue triangle down O in He:CO_2:70:30 at 1 atm.

Table 6: Average electron number per pixel and optimal gain for He:CO_2:70:30 and C_4H_{10} at 1 atm.

gas	He in He:CO_2:70:30	H in C_4H_{10}
electron number per pixel	171	1294
optimal gain	2800	400

B.2.4 Gain choice

To achieve the highest possible detection of the primary ionization, Gas-Electron-Multipliers (GEMs) are used to amplify the signal. The GEMs have very good rate capability and intrinsic ion feedback suppression. GEMs are also gate-less and can operate continuously. Each GEM has a gain of the order of 100 in a gas chosen adequalety. The gain has to be adapted to the amount of ionization, that the recoil we want to measure, losses. The electronic energy loss to the gas electron per centimeter can be calculated by using SRIM as illustrated in Figure B.2.4. From this curve, an average number of electrons that can reach a GEM hole can be calculated.

Since roughly a pixel is in front of two GEM holes, we can deduce the optimal gain necessary to be above the pixel threshold. A figure-of-merit, Figure B.2.4, can be constructed that takes into account pressure, diffusion, pixel threshold and range. Table 6 summarizes the results.

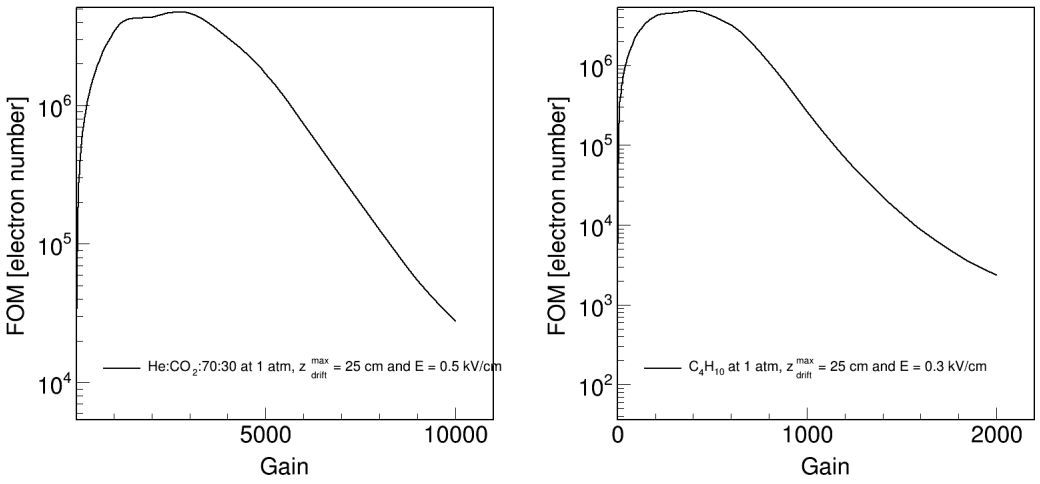

Figure 35: Gain figure-of-merit for 25 cm drift distance, 1 atm and 200 μm pixel size. Left: for He in He:CO_2:70:30. Right: for H in C_4H_{10}.

B.2.5 Pixel chip choice

There are two version of the pixel chip: FE-I3 and FE-I4. A short description can be find below.

- FE-I3
  - chip size 0.84 cm x 0.76 cm
  - pixel size 50 μm x 400 μm
  - 18 column x 160 row
  - 400 ns time range with 16 graduation
  - threshold 2215 electrons
  - 100k e^- charge range with 128 graduation
- FE-I4
  - chip size 2 cm x 1.68 cm
  - pixel size 50 μm x 250 μm
  - 80 column x 336 row
  - 1600 ns time range with 64 graduation
  - threshold 1384 electrons
  - 100k e^- charge range with 16 graduation

Table 7: Work function and mean ionization energy recorded per FE-I4 pixel for He:CO_2:70:30 and C_4H_{10} at 1 atm.

gas	He in He:CO_2:70:30	H in C_4H_{10}
Work function [eV/ion-electron-pair]	35.075	23.4
ionization energy per pixel [keV]	4.6	22

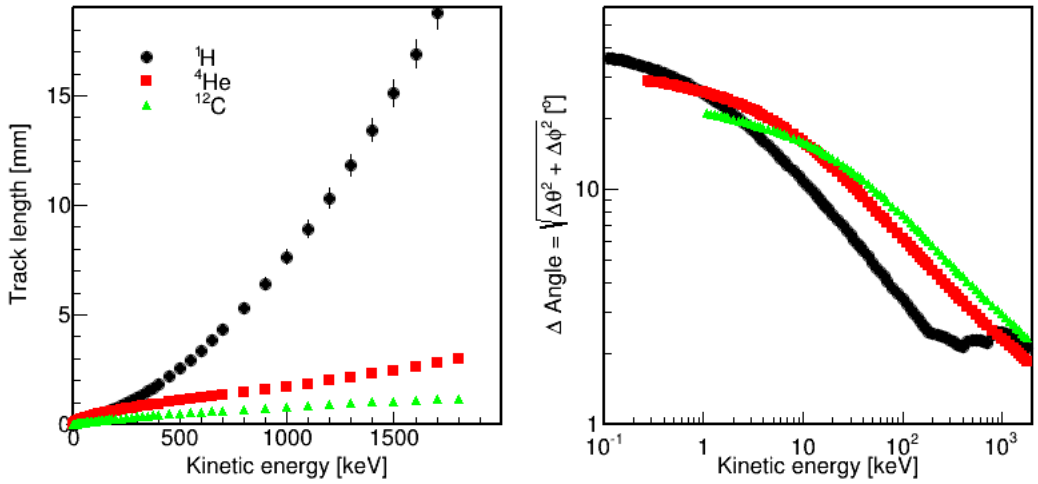

Figure 36: Left: track length versus recoil kinetic energy in C_4H_{10}. Right: angular resolution due the longitudinal and transverse straggling versus recoil kinetic energy in C_4H_{10}.

Table 6 can be converted into Table 7 which highlights the ionization energy each (FE-I4) pixel should record for He:CO_2:70:30 or/and C_4H_{10} (both at 1 atm). Even if the FE-I4 has much less charge graduation than the FE-I3 if the GEMs gain is properly chosen, the FE-I4 can reach an intrasic energy resolution of 290 eV and 1.38 keV tuned respectively for He in He:CO_2:70:30 and H in C_4H_{10}. The GEM and gas intrasic energy resolutions, roughly 20 % for both, should be added in quadrature ie total $\Delta E = 1.33$ and 6.4 keV respectively for He in He:CO_2:70:30 and H in C_4H_{10}.

If the TPC is correctly optimized the angular resolution should be dominated by the straggling as illustrated in Figures B.2.6 and B.2.5

B.2.6 Pressure and drift length choices

The pressures as well as the drift length can be optimized by determining a figure-of-merit. The pressure and the drift length figure-of-merits take into account the recoil energy spectrum due to the neutron and the directionality by considering that the diffusion effect is dominating the directionality: $L > 6.\sigma_{diffusion}(z)$ ie HT is not taken into account.

The fact that the optimum drift distance is well above 25 cm can be explained by the

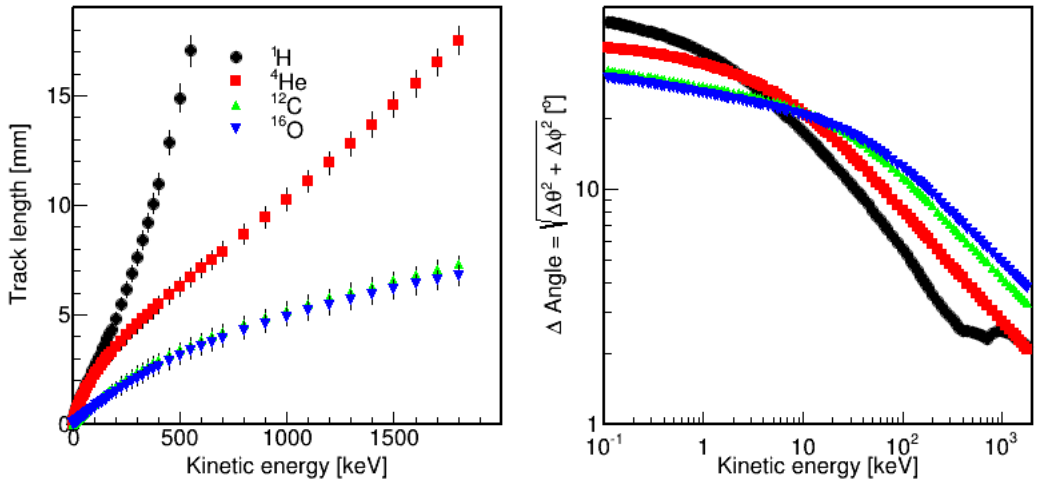

Figure 37: Left: track length versus recoil kinetic energy in He:CO_2:70:30. Right: angular resolution due the longitudinal and transverse straggling versus recoil kinetic energy in He:CO_2:70:30.

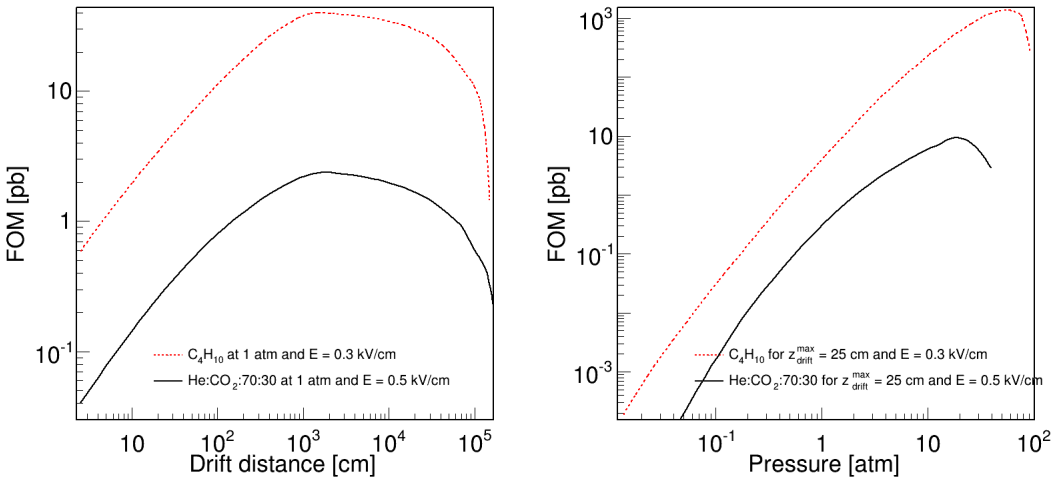

Figure 38: Left: drift distance figure-of-merit. Right: pressure figure-of-merit.

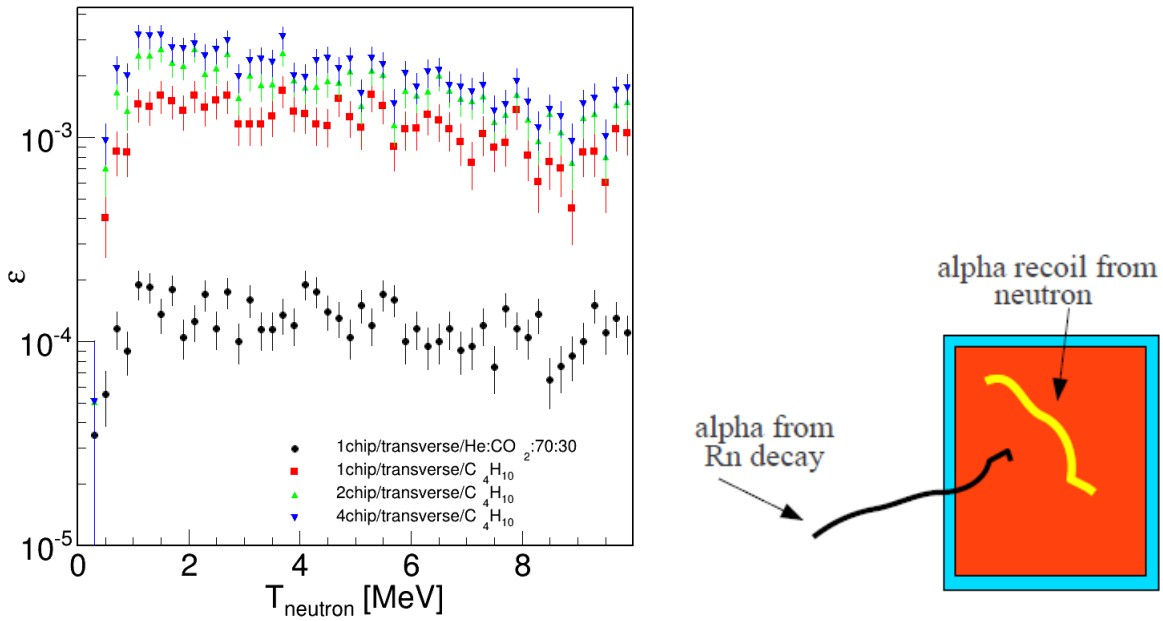

Figure 39: Left: Neutron detection efficiency as function of the neutron kinetic energy and number of pixel chip used. Right: edge cut drawing. Edge represented by the blue aera.

increase of the target volume and the long tail in the recoil energy spectrum see Figure B.2.1-bottom-left.

The iso-butane start to be liquid above 2 atm but the He:CO_2:70:30 can operate in principal at higher pressure. It should be noted that He:CO_2:70:30 $\sim$ 8 atm has the same figure-of-merit than iso-butane at 1 atm. For He:CO_2:70:30 at 8 atm, the optimum gain is 90 implying that one GEM might be enough.

B.3 Rates and Detection efficiency

Several conditions are imposed on the track to ensure that the projection of the track, with a length L, on the two-dimensionally segmented pixel chip readout plane can be exploited to extract the directionality:

- L $> 6\ \sigma_{xy}$ where σ_{xy} is the transverse diffusion
- L $> 3 \times$ GEM holes spacing
- $\Delta E_{HT} > 6\ .\ \Delta E$(E) where ΔE_{HT} is the difference in energy between the head (E_H) and the tale (E_T) and ΔE(E) the energy resolution

A so-called edge cut (Figure-right 39) is also applied to remove alpha-particle coming from natural radiation contained in the detector material and which are located outside of the

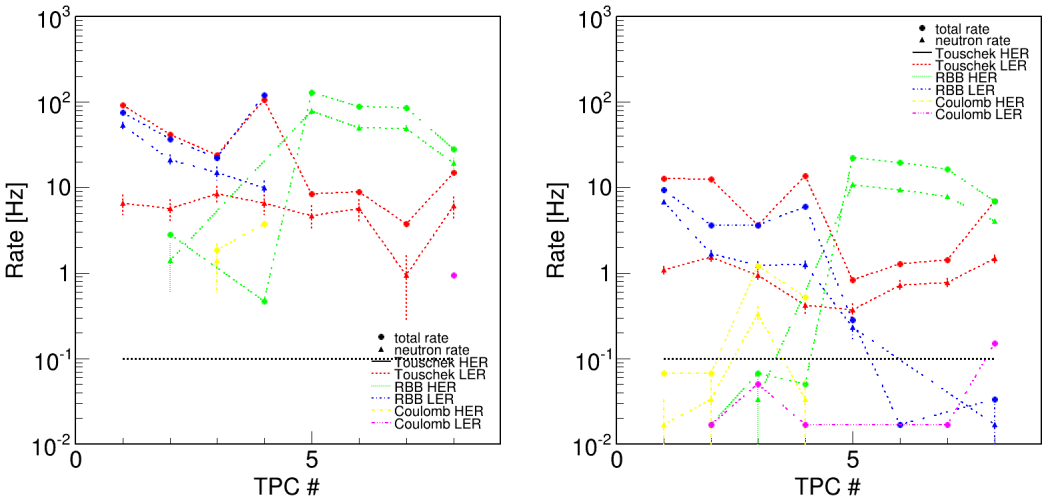

Figure 40: Rate at phase 2-phase recorded by four FE-I4 pixel chips in each TPC for the different beam-induced backgrounds. Left for C_4H_{10} at 1 atm. Right for He:CO_2:70:30 at 1 atm. The neutron rates correspond to the rate of recoil with directionality and edge cut. The total rates include all particles seen all hits recorded by the pixel chips. The black line represents the irreducible background expected.

sensitive volume. This background is critical particularly for He:CO_2:70:30 gas-mixture, since one cannot distinguish an alpha-particle recoiling due to a neutron scattering elastically on it to an alpha-particle coming from a Radon decay chain for example. The current irreducible background rate in the sensitive volume after an edge cut with the micro-DCube prototype, which used the FE-I3 pixel chip, is around 0.2 per minute. So if one considers that the irreducible background will scale with the surface then 0.2 x A(4 FE-I4) x A(1 FE-I3) ie 4.2 per minute ie roughly 0.1 Hz for the micro-BEAST-TPCs. The irreducible background is represented by a black line at 0.1 Hz in Figure 40 or by a line at 0.044 Hz (0.1 Hz x 8 TPC / 18^o) in the TPC angular plot rates: Figures 41, 42 and 43. Figure 40 shows the neutron rates with recoil exploitable directionality per TPC compared to the total rates in the TPCs.

Figures 41, 42 and 43 show the angular neutron rates for all TPCs combined with recoil exploitable directionality for the gas-mixture He:CO_2:70:30 and iso-butane both at 1 atm for the different beam-induced backgrounds.

The neutron detection efficiency as function of the neutron kinetic energy for iso-butane and the gas-mixture He:CO_2:70:30 (both 1 atm) for one, two and four FE-I4 pixel chips, Figure-left 39-left. Between one chip with gas-mixture He:CO_2:70:30 at 1 atm and four chips with iso-butane at 1 atm there is a factor ~ 8 improvement.

The neutron detection efficiency is also compared to the electron/positron and muons detection efficiencies in Figure 44.

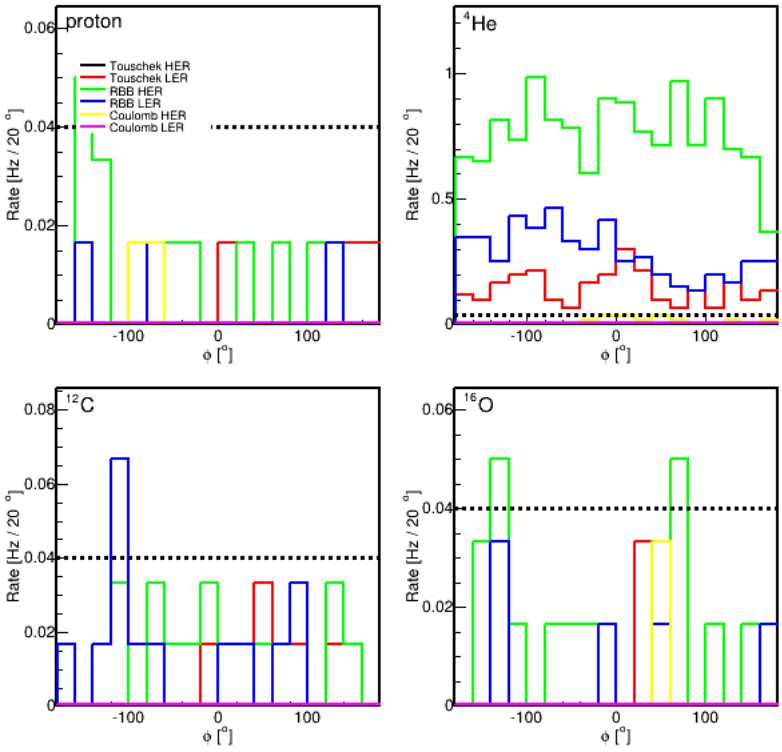

Figure 41: Rate of recoils (with directionality) versus azimuthal angle in He:CO_2:70:30 at 1 atm for the different beam-induced backgrounds at phase 2 and for all TPCs combined. Top-left: proton knock off from the detector materials. Top-right: He recoil. Bottom-left: carbon recoil. Bottom-right: oxygen recoil.

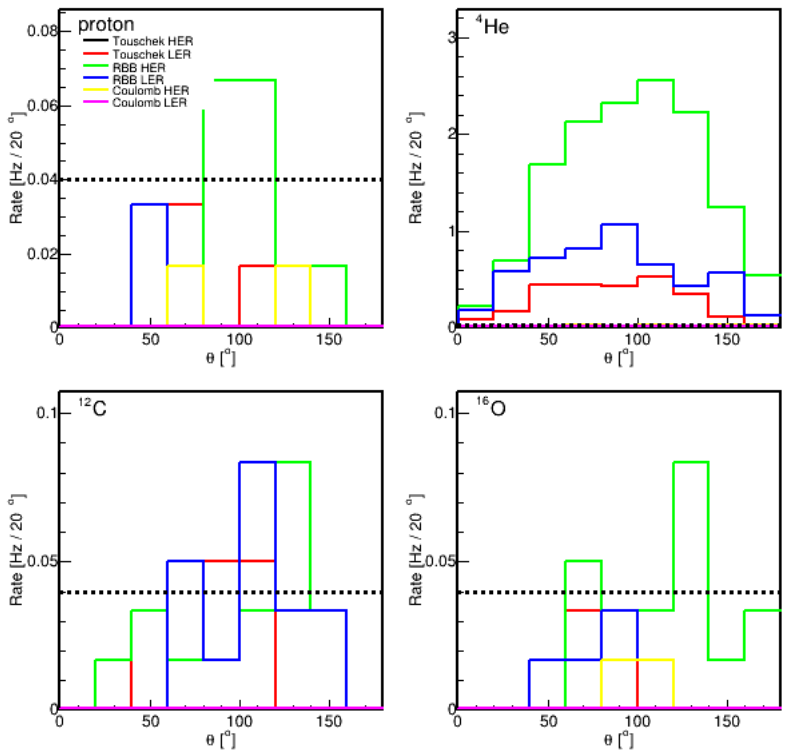

Figure 42: Rate of recoils (with directionality) versus polar angle in He:CO_2:70:30 at 1 atm for the different beam-induced backgrounds at phase 2 and for all TPCs combined. Top-left: proton knock off from the detector materials. Top-right: He recoil. Bottom-left: carbon recoil. Bottom-right: oxygen recoil.

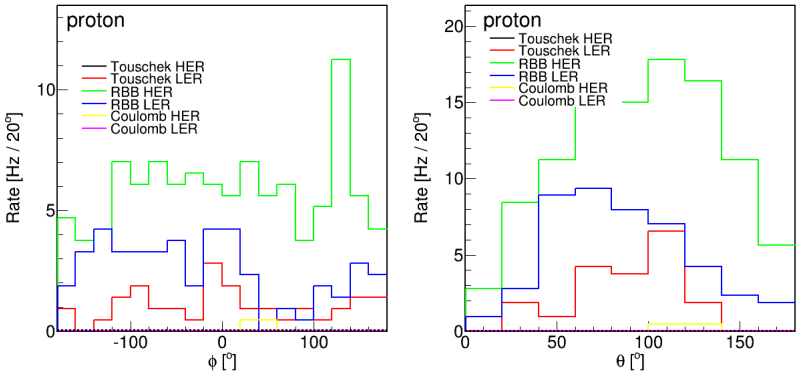

Figure 43: Rate of proton recoils (with directionality) in C_4H_{10} at 1 atm for the different beam-induced backgrounds at phase 2 and for all TPCs combined. Left: rate versus azimuthal angle. Right: rate versus polar angle.

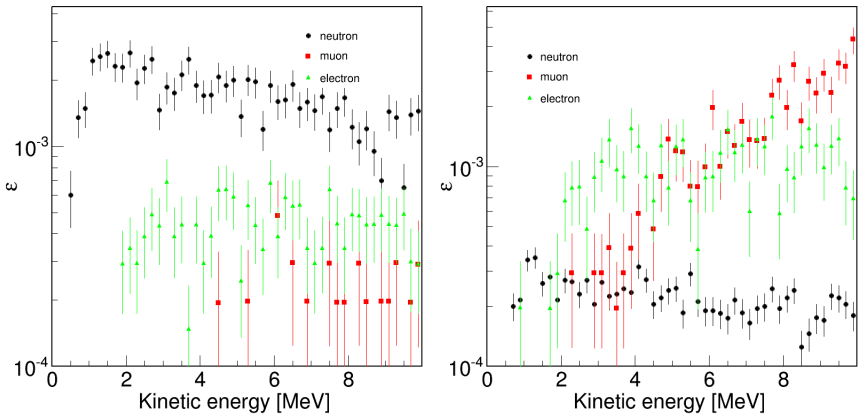

Figure 44: Detection efficiency of neutron, electron/positron and muons as function of the kinetic energy and number of pixel chip used. Left: for He:CO_2:70:30 at 1 atm. Right: for C_4H_{10} at 1 atm.

The relatively large rates due to electromagnetic particles will not be a problem as shown in Figure 45 since it can rejected during the data analysis by applying a cut on the quantity L / E where L is the track length and E the ionization energy.

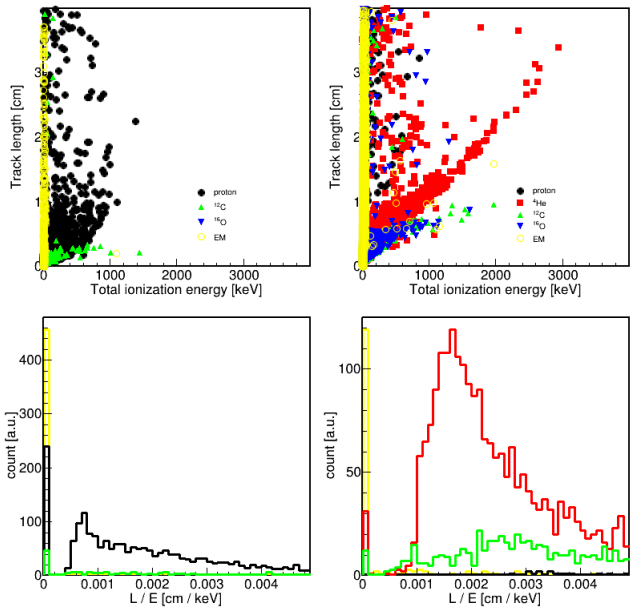

Figure 45: Top row: track length versus total ionization energy. Bottom row: L / E. Left column: C_4H_{10} at 1 atm. Right column: He:CO_2:70:30 at 1 atm.

B.4 Commissioning Detector: Beam Background Dose Estimates

	Total Dose (rad)	EM Dose (rad)	Neutron Dose (rad)
CoulombHER	0	0	0
CoulombLER	0.027	0.026	0.0010
RBBHER	0.384	0.375	0.0081
RBBLER	0.076	0.070	0.0024
TouschekHER	0.044	0.043	0.0007
TouschekLER	0.121	0.118	0.0029
Total	0.649	0.633	0.0151

Table 8: *Expected dose in the electromagnetic calorimeter from beam backgrounds, per month of running at SuperKEKB design luminosity, at a vacuum pressure of* $10^{-}9$ *Torr (simulation). In the 20* μs *simulated there was no ECL dose from beam-gas Coulomb events originating in the HER.*

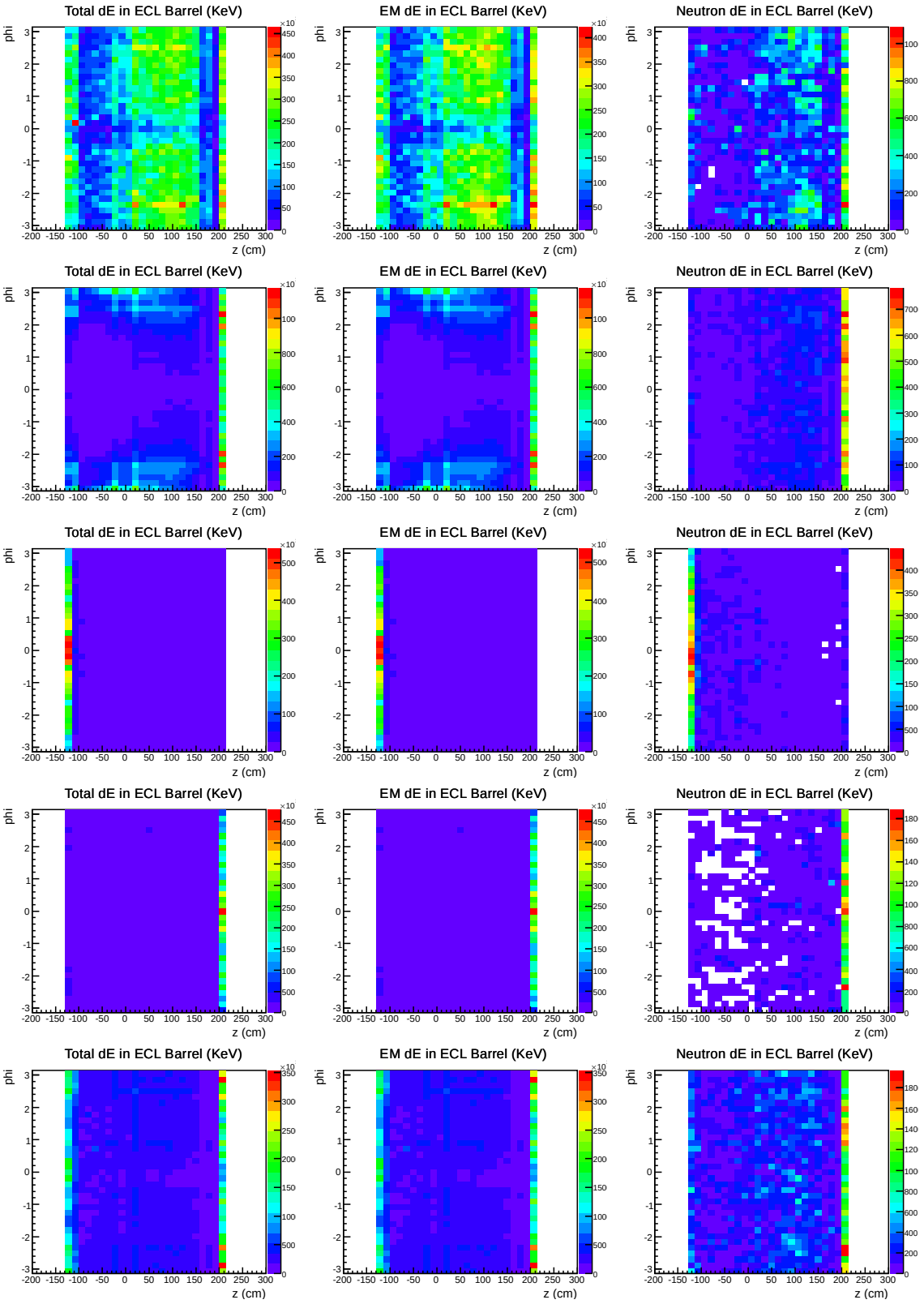

Figure 46: *Distribution of energy deposited in the electromagnetic calorimeter (ECL) from Radiative Bhabha Events, Beam-Gas Coulomb Events, and Touschek Scattering in 20 μs at SuperKEKB design luminosity (simulation). Backgrounds originating from the positron low-energy ring (LER) and electron high-energy ring (HER) were simulated and are hence*

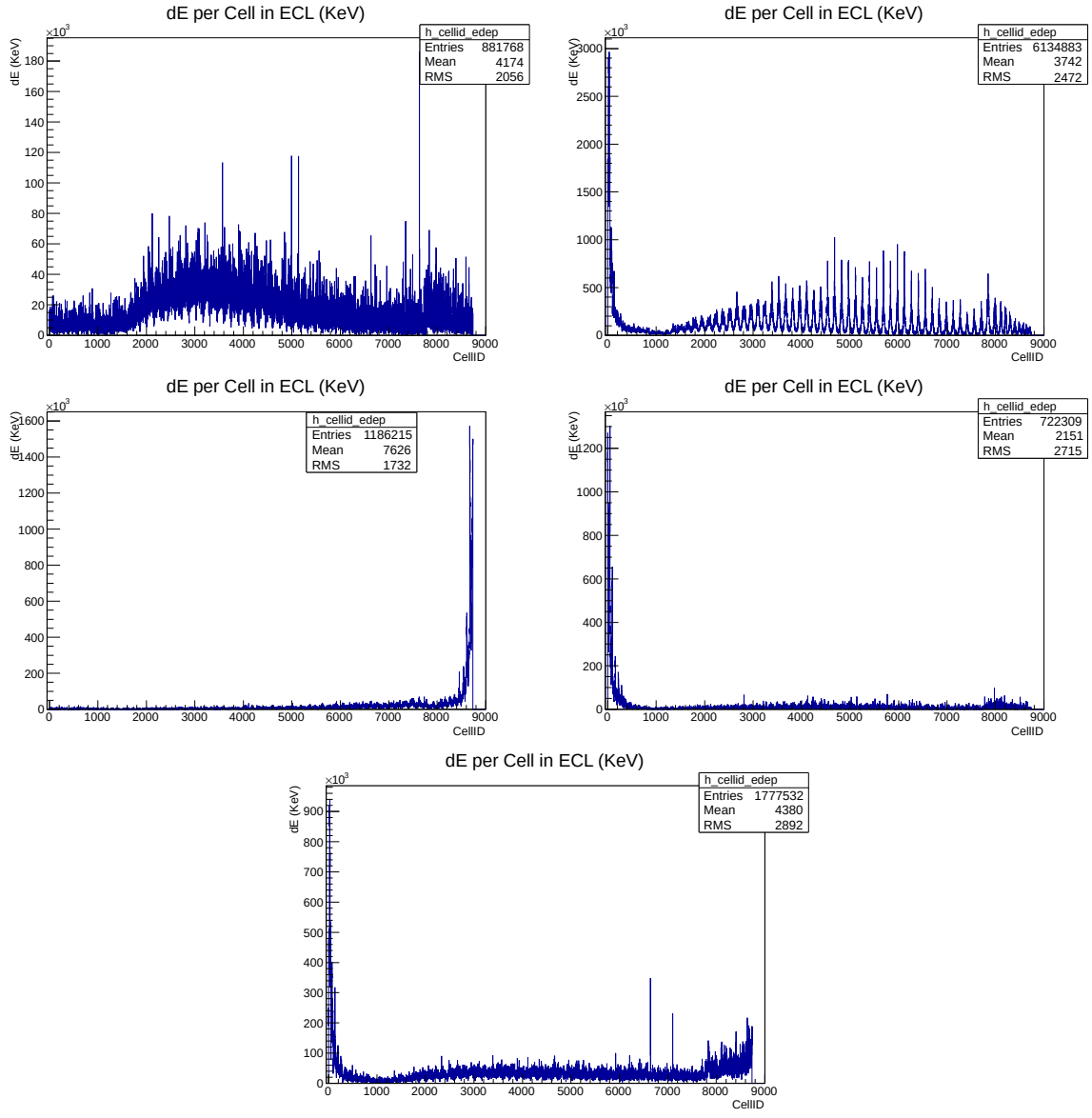

Figure 47: *Energy deposited versus electromagnetic calorimeter (ECL) crystal ID number, for Radiative Bhabha Events, Beam-Gas Coulomb Events, and Touschek Scattering, in 20 μs at SuperKEKB design luminosity (simulation). Backgrounds originating from the positron low-energy ring (LER) and electron high-energy ring (HER) were simulated and are hence plotted separately. In the 20 μ simulated there was no ECL dose from Beam-Gas Coulomb Events originating in the HER.*

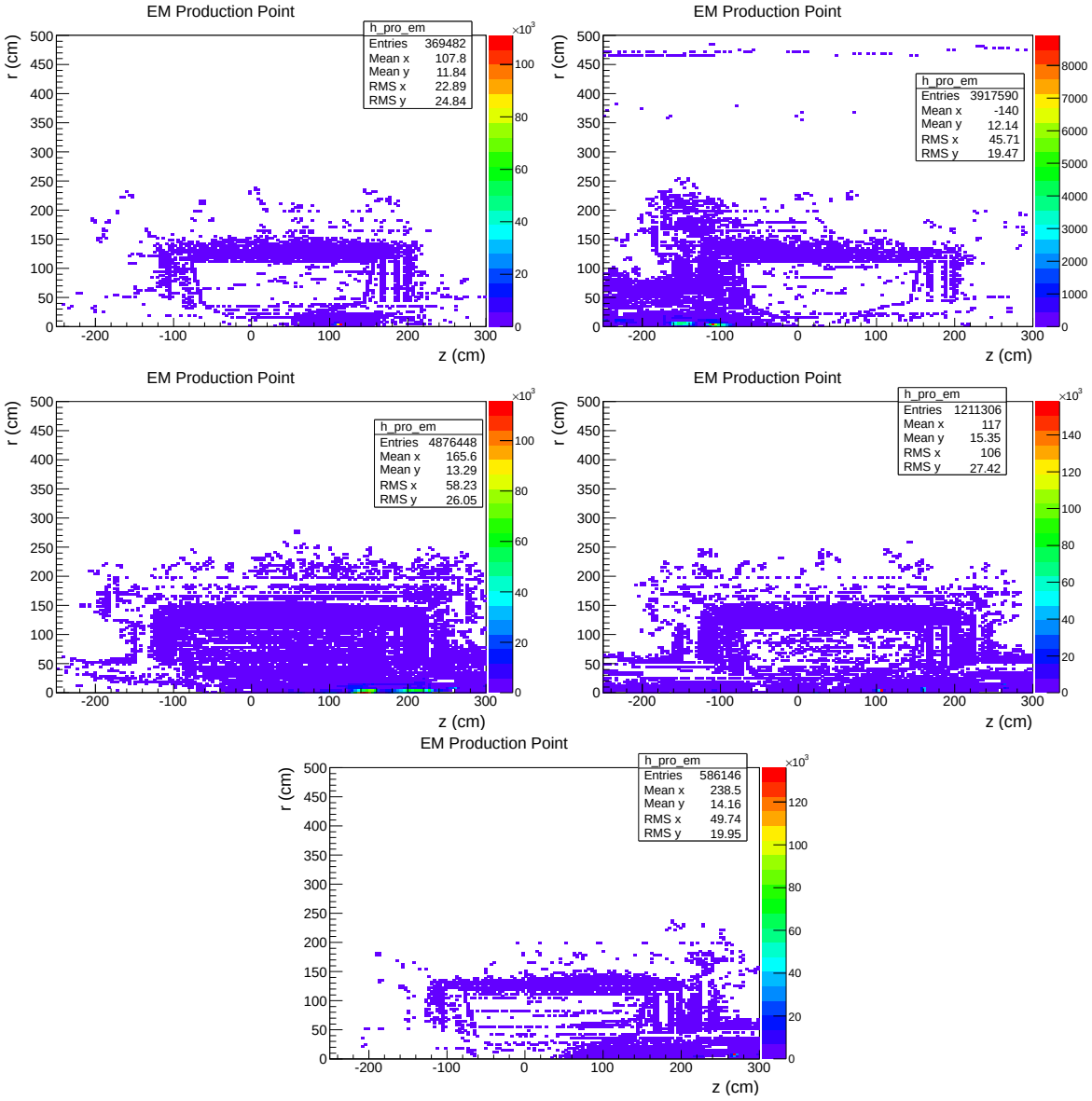

Figure 48: *Production point of EM radition for Radiative Bhabha Events, Beam-Gas Coulomb Events, and Touschek Scattering, in 1 μs at SuperKEKB design luminosity (simulation). Backgrounds originating from the positron low-energy ring (LER) and electron high-energy ring (HER) were simulated and are hence plotted separately. In the 1 μ simulated there was no ECL dose from Beam-Gas Coulomb Events originating in the HER.*

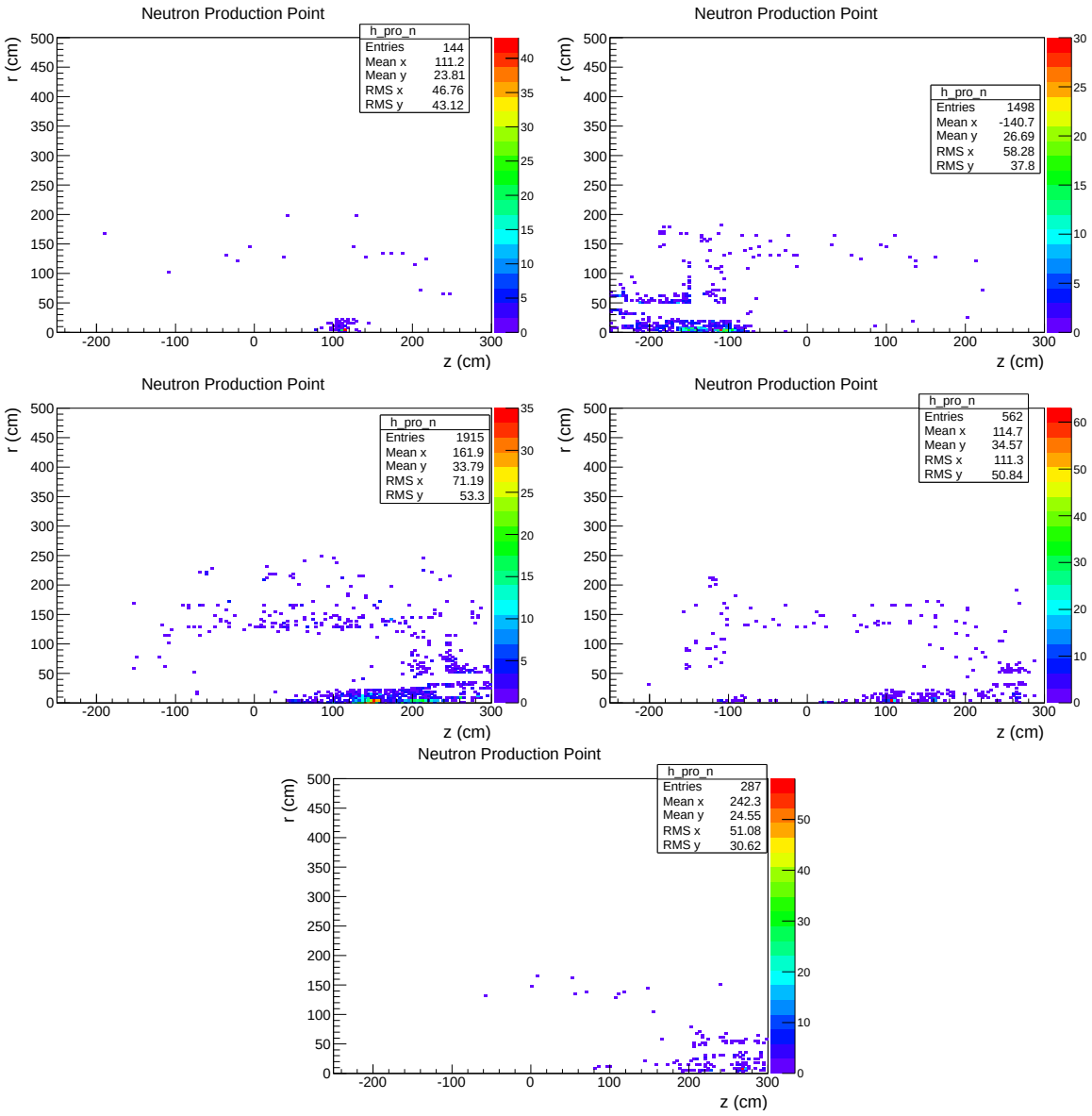

Figure 49: *Production point of neutrons for Radiative Bhabha Events, Beam-Gas Coulomb Events, and Touschek Scattering, in 1 μs at SuperKEKB design luminosity (simulation). Backgrounds originating from the positron low-energy ring (LER) and electron high-energy ring (HER) were simulated and are hence plotted separately. In the 1 μ simulated there was no ECL dose from Beam-Gas Coulomb Events originating in the HER.*

B.5 Commissioning Detector: Neutron Simulations

	Rate in backward TPCs (MHz)	Rate in forward TPCs (MHz)
Touschek LER	0.8	0.35
Touschek HER	0.3	0.01
Coulomb LER	0.75	0.15
Radiative Bhabha LER	0.25	2.35
Radiative Bhabha HER	2.7	0.3

Table 9: *Predicted rate of neutrons traversing the backward and forward micro-TPC arrays, at design luminosity.*

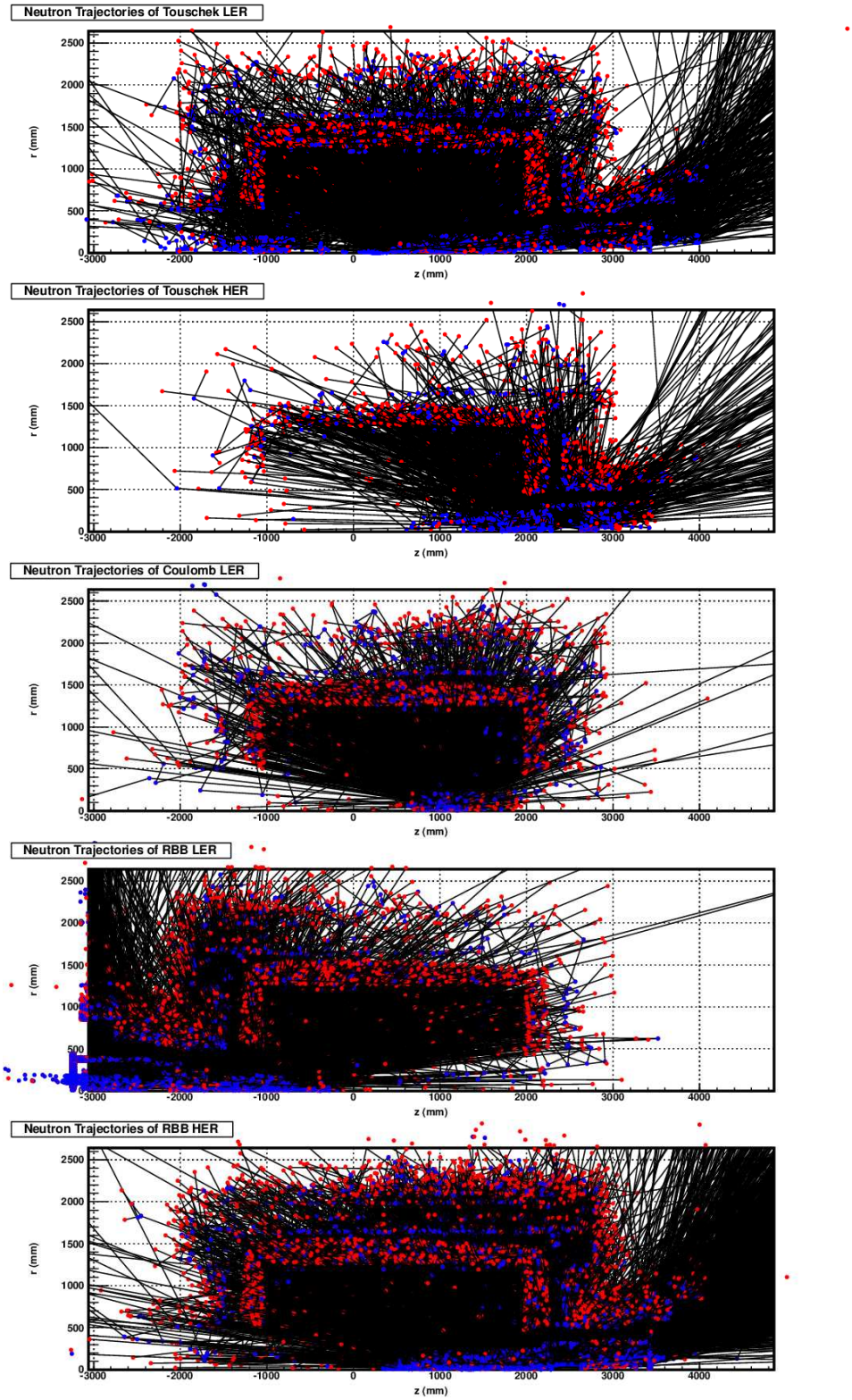

Figure 50: *GEANT production points (blue), GEANT decay points (red), and trajectories (black) of neutrons that deposit energy in the Calorimeter.*

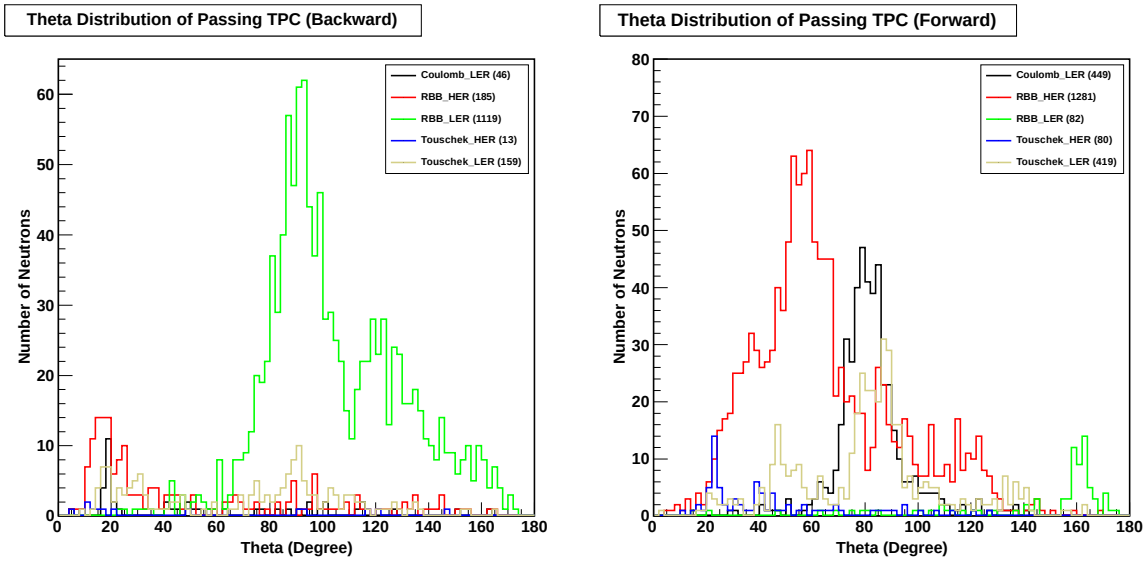

Figure 51: *Polar angle of neutrons that pass through the backward (left) and forward (right) array of microTPCs. The angle plotted is the polar angle of the incoming neutron neutron direction, as seen by each microTPC.*

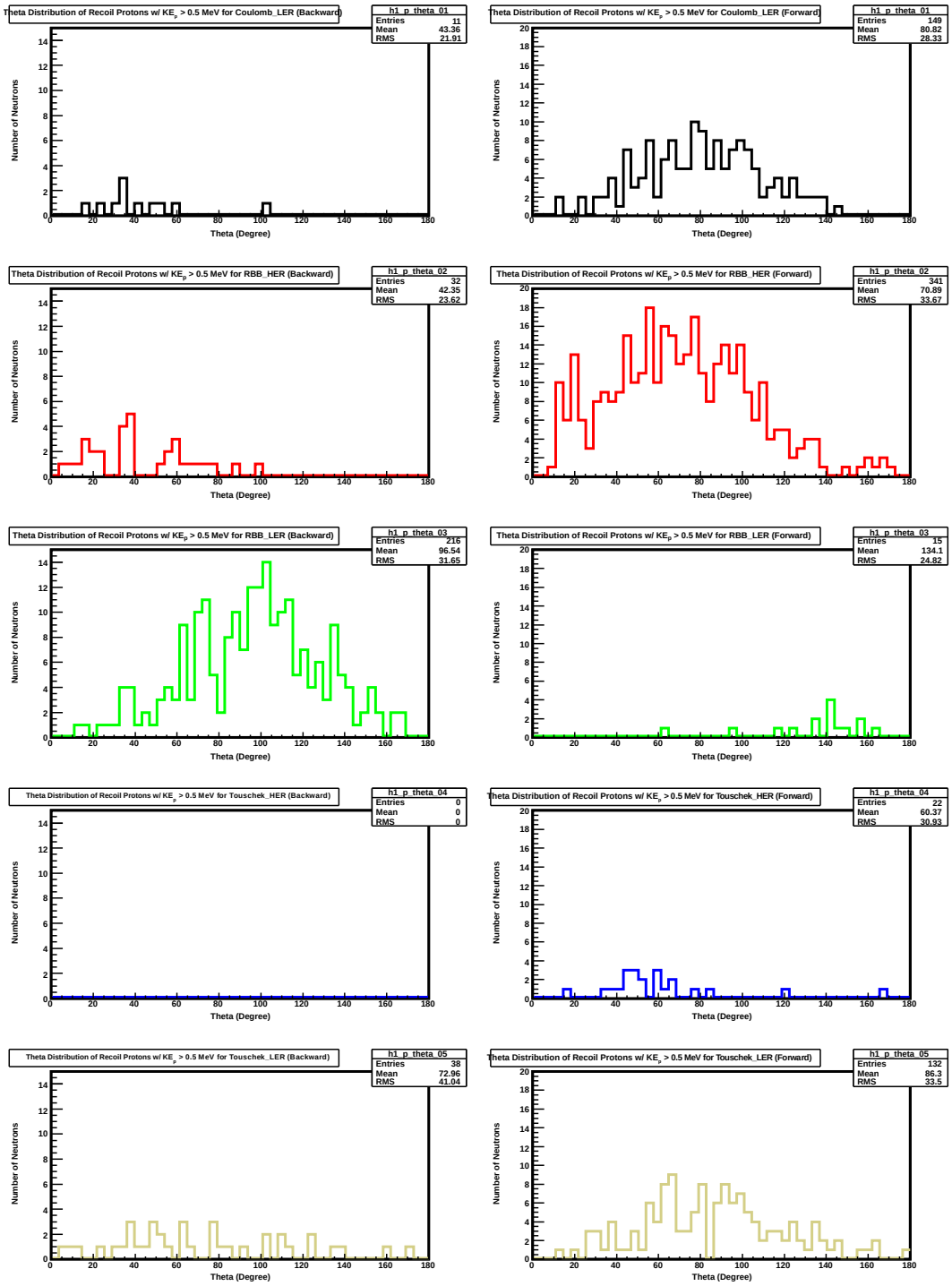

Figure 52: *Polar angle of proton recoils with $E > 500$ keV, from elastic neutron scattering in the backward (left) and forward (right) array of microTPCs. This is what we would expect to observe in the detector with a Hydrogen-based target gas.*

gas mixture	Ar:CO2 (70:30)	He:CF4 (70:30)	He:CO2 (70:30)	iso-C4H10 (100)	He:CH4 (70:30)
field strength simulated (V/cm)	1.0	1.0	1.0	2.0	1.0
drift velocity (μm/ns)	8.9	85	8.7	46.4	71.3
transverse diffusion ($\mu m/\sqrt{(cm)}$)	86.3	57	86.2	107	218.8
longitudinal diffusion ($\mu m/\sqrt{(cm)}$)	86.3	76	87.3	86	141.5

Table 10: Key parameters of candidate TPC gas mixtures.

B.6 Commissioning Detector: Micro-TPC Simulations

Candidate target gases for the micro-TPCs are: $He : CF_4$, $He : CO_2$ and iso-C_4H_{10}, and $He : CH_4$. Helium and Hydrogen-based target gases are best for neutron detection, and the light target atoms maximize energy transfer during elastic scattering. An addition, we typically use $Ar : CO_2$ for prototype studies and calibration. This section summarizes they key performance parameters of these candidate gases, which were used to arrive at the micro-TPC specification in the commissioning detector CDR.

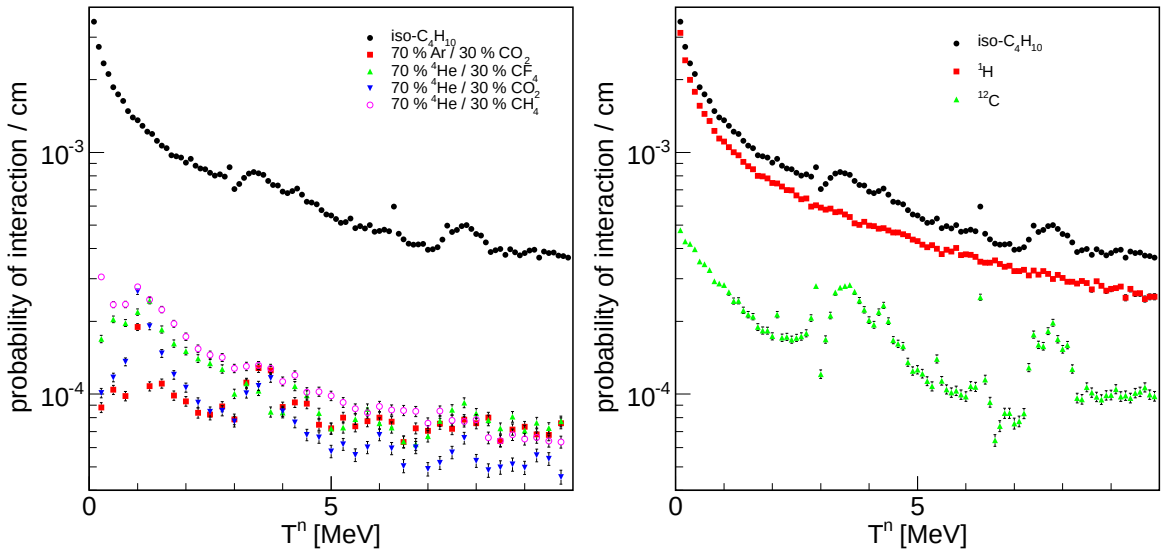

Figure 53: *Probability of neutron scattering per cm of target gas, at atmospheric pressure and room temperature. Below 2-MeV, the scattering is almost exclusively elastic. The effiency of iso-C4H10 is an order of magnitude higher than that of other candidate gases, simply because there are 10 hydrogen atoms per molecule. Hydrogen is also better than Helium for maximizing energy exchange during scattering, and in that the scattering probability for the target nucleus (Hydrogen) is significantly higher than that of other nuclei in the gas. The drawback of working with hydrogen-based gas mixtures is safety - they tend to be flammable.*

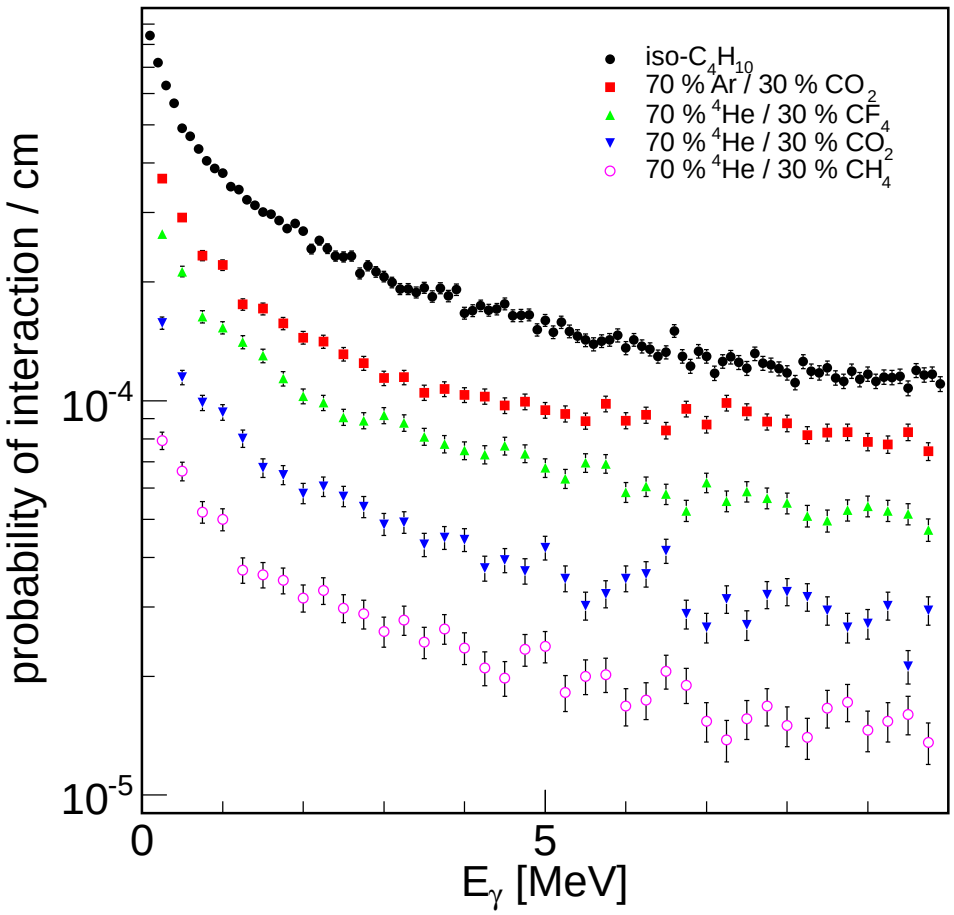

Figure 54: *Probability of gamma-ray scattering per cm of target gas, at atmospheric pressure and room temperature.*